NASA TECHNICAL NOTE

NASA TN D-4512

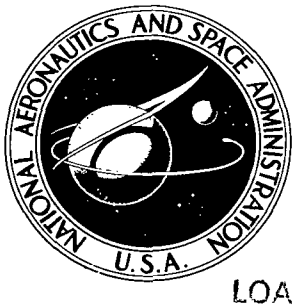

NAVIGATION AND GUIDANCE ANALYSIS OF A MARS PROBE LAUNCHED FROM A MANNED FLYBY SPACECRAFT

by Thomas B. Murtagh, Flora B. Lowes, and Victor R. Bond

Manned Spacecraft Center
Houston, Texas

NATIONAL AERONAUTICS AND SPACE ADMINISTRATION • WASHINGTON, D. C. • APRIL 1968

NAVIGATION AND GUIDANCE ANALYSIS OF A MARS PROBE LAUNCHED FROM A MANNED FLYBY SPACECRAFT

By Thomas B. Murtagh, Flora B. Lowes,
and Victor R. Bond

Manned Spacecraft Center
Houston, Texas

NATIONAL AERONAUTICS AND SPACE ADMINISTRATION

For sale by the Clearinghouse for Federal Scientific and Technical Information
Springfield, Virginia 22151 – CFSTI price $3.00

ABSTRACT

The navigation and guidance analysis of a Mars probe launched from a manned flyby spacecraft is presented in this paper. This study was initiated with the probe and spacecraft separation at the Mars sphere of influence and was terminated with the probe arrival at a specified entry altitude and the spacecraft arrival at Mars periapsis. The disclosures of the study indicate that the results are decidedly dependent on the initial spacecraft errors at the time of separation and on the system model errors assumed when processing navigation data.

NAVIGATION AND GUIDANCE ANALYSIS OF A MARS PROBE LAUNCHED FROM A MANNED FLYBY SPACECRAFT

By Thomas B. Murtagh, Flora B. Lowes,
and Victor R. Bond
Manned Spacecraft Center

SUMMARY

The navigation and guidance analysis of a Mars probe possibly to be launched from a manned spacecraft during Mars flyby missions in 1975 and 1976 is presented. The study is initiated with the probe and spacecraft separation at the Mars sphere of influence and is terminated with the probe arrival at a specified entry altitude and the spacecraft arrival at Mars periapsis. The relative state between the probe and spacecraft is assumed to be perfectly known so that the uncertainty covariance matrix for the probe is equivalent to that of the spacecraft. The spacecraft position and velocity uncertainties are reduced by processing onboard sextant or theodolite measurements with a Kalman filter. The results of the study indicate that spacecraft periapsis-altitude dispersions between 1 and 6 n. mi. can be obtained with one or two midcourse velocity corrections totaling between 10 and 150 fps depending on (1) Mars radius uncertainty; (2) instrument accuracy; (3) sighting frequency; (4) type, number, and timing of corrections; and (5) the accuracy of their execution. The probe entry flight-path-angle dispersions ranged from 0.13° to 0.21° for the same range in velocity-correction-vector magnitude and for the same parameter variations as indicated for the spacecraft.

INTRODUCTION

Consideration is being given to the possibility of launching a Mars probe from a manned spacecraft during a Mars flyby mission between 1975 and 1980. Such a probe could be manned or unmanned. Basically, the probe must have the ability to land on the Martian surface and, after a stay time consistent with mission constraints, to launch and to rendezvous with the flyby spacecraft.

The design of such a probe is influenced by many factors, not the least of which is the fuel required to complete the mission safely. The fuel required is, in turn, a function of many other parameters, such as (1) navigation system accuracy; (2) type and number of navigation measurements processed; (3) dispersions and uncertainties in the spacecraft trajectory at the time of separation; (4) type, number, and timing of midcourse velocity corrections and the accuracy of their execution; (5) distance from Mars when the probe is separated from the spacecraft; and (6) leadtime of the probe landing with respect to spacecraft periapsis passage.

These last two parameters primarily affect the separation velocity of the probe with respect to the spacecraft. For a given leadtime, the separation velocity is approximately an inverse linear function of the distance from the planet; for a specified separation distance, the separation velocity is proportional to the leadtime required.

To simplify the analysis of the probe-and-spacecraft navigation and guidance systems, the separation distance and the leadtime were fixed so that the probe would separate from the spacecraft at the Mars sphere of influence (SOI) and land on the Martian surface 1 hour ahead of the spacecraft periapsis passage. The relative state between the probe and the spacecraft was assumed to be known perfectly so that the uncertainty covariance matrices computed for the probe and the spacecraft were equal. The spacecraft position and velocity uncertainties were reduced by onboard processing of sextant or theodolite optical measurements using a Kalman filter. The study was initiated with the probe and spacecraft separation and was terminated with the probe arrival at a specified entry altitude and the spacecraft arrival at Mars periapsis.

The purpose of the study is to present the midcourse root-mean-square (rms) velocity corrections required for the probe to attain certain flight-path-angle dispersions at entry (with corresponding vacuum periapsis-altitude dispersions) and for the spacecraft to attain reasonable altitude dispersions at the periapsis of the flyby hyperbola. In the first section of the paper, the assumptions made in the study are discussed, followed by a section dealing with the reference trajectories used in the analysis. Next, a description of the navigation and guidance systems of the probe and flyby spacecraft is presented with a subsequent discussion of the digital computer program used to generate the results. The results and discussion section presents the navigation and guidance data in separate sections, further subdivided into discussions of either the probe or the spacecraft navigation and guidance systems. The pertinent mathematical developments are relegated to appropriate appendixes.

The authors gratefully acknowledge the efforts of L. S. Cicolani of the NASA Ames Research Center in the generation of the covariance matrices presented in table I in this paper and wish to thank B. J. Garland of the NASA Manned Spacecraft Center for permission to reproduce figure 1 and for suggesting the launch dates and trip times used.

SYMBOLS

$A(t)$	transformation matrix
a	semimajor axis
B	6-by-3 matrix defined by equation (C5)
$C(\alpha X^2), S(\alpha X^2)$	Battin's auxiliary functions (The values of X are defined in eqs. (B25) and (B26).)
c	ratio of planet-radius error to the radius of the observed planet

$E, E(t)$	covariance matrix of state-vector uncertainty
E_E, E_0	eccentric anomalies at entry and separation, respectively
e	eccentricity
f	true anomaly angle
$G(t)$	6-by-6 guidance matrix
$G_1(t), G_2(t)$	3-by-3 submatrices of guidance matrix
$H, H(t)$	sensitivity matrix
H_E, H_0	hyperbolic equivalent of eccentric anomaly at entry and separation, respectively
h	altitude
I	identity matrix
i	inclination angle
$K(t)$	weighting matrix
$L(t)$	3-by-3 matrix defined by equation (C8)
$\ell(t)$	scalar defined by equation (C9)
$M(t)$	matrix defined by equation (A11)
$N(t)$	covariance matrix of velocity-correction error
$P(t)$	matrix defined by equation (C10)
p	semilatus rectum
Q	the measurable, as defined in equation (A1) ($Q = \beta$ for sextant measurement)

$R = \sqrt{x^2 + y^2 + z^2}$ in equation (A6)

$R' = \sqrt{x^2 + y^2}$ in equation (A6)

$R(t)$	covariance matrix of measurement errors

$\underline{r}$	position vector
r_p	planet radius
$\underline{s}$	state vector (position and velocity)
T	nominal time of arrival at target (or fixed terminal time)
T_π	nominal time of periapsis passage
t	time
$\underline{u}( )$	unit vector in the direction of ( )
v_H	down-range speed
$\underline{v}$	velocity vector
$W, W(t)$	matrix defined by equation (A8)
$\underline{W}$	vector defined by equation (D20)
$X(t)$	covariance matrix of state-vector dispersion
x, y, z	components of the vector from the vehicle to the observed body
$\underline{y}_1$	gradient of periapsis radius with respect to position
$\underline{y}_2$	gradient of periapsis radius with respect to velocity
$\underline{Z}(t)$	gradient vector defined by equation (E6)
$\underline{Z}_1$	gradient of flight-path angle with respect to position
$\underline{Z}_2$	gradient of flight-path angle with respect to velocity
α	reciprocal of semimajor axis
α_0	right ascension
β	star-planet included angle (sextant)
β_1, β_2	celestial latitude and longitude of observed planet as viewed from spacecraft (theodolite)
γ	flight-path angle

$\Delta\underline{v}$	velocity-correction vector
$\Delta\gamma$	probe entry flight-path-angle dispersion
δ_0	declination
$\overline{\epsilon^2}$	mean-squared engine-cutoff error
$\overline{\zeta^2}$	mean-squared error in thrust-vector magnitude
$\overline{\eta^2}$	mean-squared error in thrust-vector orientation
θ	angle defined by equation (A12)
μ	gravitational constant multiplied by the mass of the central body
σ	parameter defined by equation (B14)
σ_B^2	sensor bias variance
σ_I^2	sensor variance
σ_T^2	total variance of observation errors
$\phi(t, t_0)$	state-transition matrix evaluated between t and t_0
ϕ_{11}, ϕ_{12} ϕ_{21}, ϕ_{22}	3-by-3 submatrices of the state-transition matrix
Ω	right ascension of ascending node

Subscripts:

d	dispersion
E	entry
F	fixed time of arrival
h	normal to the trajectory plane (in eq. (B9))
nom	nominal

p	planet
R	required
r_0	initial position
s	star
$\underline{s}$	state (eq. (A1))
T	terminal time
u	uncertainty
V	variable time of arrival
vh	vehicle-horizon
vp	vehicle-planet
w	trajectory plane
ϵ	estimate
π	periapsis

Superscripts:

T	transpose
-1	inverse
+	value after measurement or correction
-	value before measurement or correction

Operators:

$\delta( )$	variational operator (small deviation from reference value)
$\xi( )$	expected value
$\nabla_{\underline{s}}( )$	gradient with respect to $\underline{s}$

ANALYSIS

Assumptions

The following ground rules are postulated for the analysis presented in this paper.

1. The probe and the spacecraft are separated at the Mars SOI, with the probe landing approximately 1 hour prior to spacecraft passage through periapsis.

2. Two sets of representative spacecraft uncertainty and dispersion covariance matrices at the Mars SOI were generated by propagating and updating an Earth-injection covariance matrix with rms position-and-velocity errors of 4 n. mi. and 16 fps. The first set, presented in table I(a), used only Earth-based radar range and range-rate tracking data to update the spacecraft uncertainty matrix, and the second set, presented in table I(b), used a combination of Earth-based and onboard navigation data to update the spacecraft uncertainty matrix during the Earth-to-Mars portion of the mission. A more detailed description of the systems used to generate these matrices can be found in reference 1.

3. The reference trajectories used were assumed to be ideal conics, and the state-transition matrix used to propagate the errors was derived analytically for two-body conic trajectories.

4. The relative state between the probe and the spacecraft is perfectly known so that the uncertainty covariance matrices of the probe and spacecraft are equivalent. The spacecraft covariance matrix is updated by processing onboard sextant or theodolite measurements with a Kalman filter.

5. The total-variance equation of the observation errors is written as

$$\sigma_T^2 = \sigma_I^2 + (c \tan \theta)^2 + \sigma_B^2 \tag{1}$$

where σ_I is the standard deviation of the instrument error (equals 5 arc seconds) and σ_B is the standard deviation of instrument bias (equals 60 arc seconds). The parameter c is defined as the ratio of planet-radius uncertainty to the planet radius; the values used in this paper were 0.001 and 0.01 (corresponding to Mars-radius errors of 2 and 20 n. mi., respectively). The derivation and discussion of this equation are given in appendix A.

6. Fixed time of arrival (FTA) guidance and variable time of arrival (VTA) guidance were used to compute the rms velocity corrections and appropriate target dispersions for both the probe and the spacecraft. No attempt was made to optimize the velocity-correction schedule for either of these types of guidance.

7. A summary of navigation and guidance errors is presented in table II.

The Trajectory Characteristics

The study is performed for the two Mars flyby launch opportunities of September 20, 1975, and April 17, 1976. These trajectories will be designated as the short-long and the long-short cases, respectively. The trajectory characteristics are summarized in table III, and their heliocentric trajectories in the ecliptic plane are presented in figures 1(a) and 1(b). These trajectories have very nearly the same total trip times (671.93 days and 680.58 days, respectively). The trajectories are chosen primarily because they require near-minimum velocities at injection from the Earth (15 150 fps and 14 050 fps, respectively). The injection velocity is equal to the difference between the perigee velocity of the escape hyperbola and the circular velocity at perigee. The perigee altitude at injection was 262 n. mi. for both cases.

Both of these trajectories have hyperbolic asymptotes at Earth departure with declinations that are within $\pm 35°$. It is pointed out in reference 2 that declinations in this range are necessary for good orbit determination with Deep Space Instrumentation Facility tracking stations. This range of declinations also permits departure trajectories with inclinations that are within the launch-azimuth (from Kennedy Space Center) safety constraints.

It is important to consider the advantage of designing the flyby-probe mission so that it can be either a short-long or a long-short mission. The opportunities for minimum injection velocities for short-long (or long-short) missions are approximately 765 days apart, but a long-short opportunity occurs 210 days after each short-long opportunity. Therefore, the long-short opportunity can be considered as a backup or alternate launch date to the short-long launch date.

The initial conditions for the flyby spacecraft at the Mars SOI were obtained by matched conic techniques. These initial conditions are presented for the short-long and long-short cases in table IV. It is interesting to note the differences between these two trajectories within the Mars SOI. For the short-long case, the spacecraft is within the Mars SOI for approximately 38 hours, has a retrograde inclination with respect to the Martian equator of approximately 144°, and has a periapsis altitude of approximately 106 n. mi. located in the northern hemisphere. For the long-short case, the spacecraft is within the Mars SOI for approximately 30 hours, has an inclination of 13°, and has a periapsis altitude of approximately 112 n. mi. located in the southern hemisphere.

The probe trajectory is computed as shown in appendix B. The initial position vector is the same as that of the flyby spacecraft at the entrance to the Mars SOI. Specifying this initial position vector, along with the entry speed, the entry flight-path angle, the entry altitude, and the inclination, completely determines the probe trajectory, except for an ambiguity in the right ascension of the ascending node. The inclination is chosen to be the same as that of the flyby spacecraft to avoid plane change. The right ascension of the ascending node is also chosen to be the same as that of the flyby spacecraft to maintain the minimum distance between the flyby spacecraft and the probe. For this study, the probe entry altitude and flight-path angle assumed were 315 000 feet and -20°. For the short-long and long-short trajectories, the entry speeds were 33 600 fps and 40 000 fps, respectively.

Description of Navigation and Guidance Systems

The pertinent navigation-system equations are developed in appendix A along with the sensitivity vector, or matrix, which relates measurement deviations to state-vector deviations for the Mars-star included-angle measurement (sextant) and the spacecraft-Mars direction-of-line-of-sight measurement (theodolite). The geometry of the sextant included-angle measurement is illustrated in figure 2; the theodolite line-of-sight-direction measurement geometry is presented in reference 3. The appropriate guidance-system error equations are developed in appendix C, and the derivation of the guidance matrix for FTA and VTA guidance is presented in appendix D. Appendix E is an outline of the procedure for computing the rms flight-path-angle dispersions or uncertainties and the radius-of-periapsis dispersions or uncertainties from the state dispersions or uncertainties.

Description of Simulation

A digital simulation program developed by the authors was used to generate the results presented in this paper. The basic components of this program are a control routine which generates trajectory and covariance-matrix time histories for both the probe and the spacecraft, a set of subroutines which compute the conic state-transition matrix for propagating errors and integrating the state vector along the conic, and another set of subroutines which update the covariance matrices as a result of a navigation measurement or a guidance maneuver. The rms position-and-velocity errors, computed from the square root of the trace of the covariance matrix, are presented in a locally level coordinate system which displays both in-plane and out-of-plane errors. The x-axis (altitude) of this coordinate system is along the radius vector to the probe or the spacecraft, the y-axis (range) is in the direction of the velocity, and the z-axis (track) is along the orbital angular-momentum vector. The errors in this system are designated as altitude, range, and track errors, and the time rates of change.

DISCUSSION OF RESULTS

Navigation Results

Uncertainties in the estimate of the state of a vehicle as determined by navigation measurements represent a lower bound for the state dispersions. It is evident from equation (C4) in appendix C that state dispersions are never better than the uncertainties in the estimate. By investigating different navigation types to reduce the estimated uncertainties, the dispersions can also be reduced. Thus, as the navigation is improved, so is the ability to guide a spacecraft to a specified target.

For navigation in the Mars-probe study, onboard optical determinations of an angle were used. Consideration was given to two optical instruments which might be used — the sextant and the theodolite. Although for parallel studies the theodolite tends to give somewhat better information than the sextant, the theodolite information was not found to be sufficiently better to justify presenting the theodolite data when the impracticability of the theodolite was considered. Thus, all data presented pertain to the star-planet included-angle measurement assumed to be made with an onboard

sextant and processed by a Kalman filter. Mars was the planet used for all measurements. However, the star used for each measurement was randomly chosen from a limited catalog of stars included in the simulation program. No attempt was made to optimize the choice of stars for the measurements.

The effect of the previously described navigation method in reducing state-position uncertainties was investigated. This effect is presented for both of the trajectories described in table III, and in each case, the observation errors of table II and the initial uncertainty matrices of table I were used. Since the instrument bias σ_B (which is included in eq. (1)) can be related to the state, it is possible to incorporate σ_B in the state array and to have the filter act on it. Through this action, the bias could be reduced; consequently, the effect of the bias on the estimated uncertainties would be lessened. Only the instrument bias, not the basic instrument error, was estimated by this technique. The purpose of this estimation was to attempt to model errors which contribute to the overall error in estimating the state.

Since the position uncertainty of principal interest is at periapsis for the spacecraft and at vacuum periapsis for the probe, the results of the analysis are presented for those terminal points only.

From previous studies, it has been found that a measurement frequency of less than 30-minute intervals does not significantly affect the periapsis position-error curve profile. Thus, the results presented are for measurement intervals of 30 minutes. Results of the navigation analysis are presented in figures 3 and 4.

Spacecraft. - Figure 3 shows the spacecraft rms altitude uncertainties at Mars periapsis. These values are plotted against the time to Mars periapsis to illustrate approximately how well the periapsis-altitude uncertainty is known at any time along the trajectory.

Figures 3(a) to 3(d) each contain four curves. The two solid-line curves represent the rms periapsis-altitude uncertainty for a planet-radius error of approximately 2 n. mi. (or $c = 0.001$), and the two broken-line curves represent the rms periapsis-altitude uncertainty for a planet-radius error of approximately 20 n. mi. (or $c = 0.01$). Of the two curves for each specified radius error, one curve represents the effect of the inclusion of instrument bias in the error model, and the other curve represents the effect of no instrument bias. The curves are marked accordingly.

Figures 3(a) and 3(b) pertain to the short-long trajectory for two different sets of initial errors. The initial errors $E(t_0)$ and $X(t_0)$, represented in figure 3(a), were generated from Earth-based radar tracking only. Those errors represented in figure 3(b) were generated from the combination of Earth-based radar and onboard tracking. It is evident from these two figures that the combination of Earth-based radar and onboard tracking gives lower initial uncertainties at the Mars SOI. Because of these lower initial uncertainties, those uncertainties computed for the time from the Mars SOI to Mars periapsis produce initially lower and continually smoother curve profiles than those produced by the initial errors generated from radar tracking alone. However, the curves of both figures tend to converge to approximately the same four respective terminal values.

Figures 3(c) and 3(d) show the same curves as in figures 3(a) and 3(b) when generated for the long-short trajectory. Practically the same conclusions can be drawn from these two figures as from figures 3(a) and 3(b). The slight differences in the profiles of the curves and in the initial uncertainties are the result of the shorter time span of the trajectory between the Mars SOI and the Mars periapsis.

For the respective case of interest, the effect of the calculation of spacecraft uncertainties can be determined from any of these four figures when a small planet-radius error of 2 n. mi. or a large planet-radius error of 20 n. mi. is considered. Also evident in the figures is the effect of including an instrument bias in the error model with either of the two assumed radius errors. For the first few hours of navigation measurements, the instrument bias has the effect of keeping the uncertainty curve profiles from being lowered; this is followed by a general smoothing-off effect which is a result of the filter in the state estimation of the bias and of the tendency of the filter to decrease the initial included bias value. It is possible to estimate the planet-radius error in a similar manner, but this was not included in the study. Because of the relation between the estimated uncertainties and the state dispersions, which was previously pointed out, the study of the uncertainty curve profiles of figure 3 can aid in determining correction times.

Probe. - Figure 4 pertains to the probe and presents the rms altitude uncertainties at vacuum periapsis for the short-long and long-short trajectories, respectively, and, also, the two types of initial errors in each case. The parts of figure 4(a, b, c, and d) are presented in the same manner and sequence as the parts of figure 3 so that conclusions concerning the varying conditions may be drawn for the probe at vacuum periapsis in the same manner as for the spacecraft as the flyby-hyperbola periapsis.

The initial projected probe-altitude uncertainties are slightly higher in value than the corresponding initial projected spacecraft uncertainties because of the degradation at separation in the covariance matrix $E(t_0)_{PROBE}$ which results from an imperfect velocity correction execution. This degradation is evident from equation (C3). The degrading effect is noticeable in the probe uncertainty curves for the complete time span. However, the profiles of the curves of figures 3 and 4 are so similar that it is possible to draw approximately the same conclusions for the probe as for the spacecraft.

Guidance Results

Spacecraft. - A representative set of spacecraft guidance data is summarized in table V for the short-long and long-short trajectories and for the two sets of initial uncertainty and dispersion matrices presented in table I. In the data presented, it was assumed that biased sextant-navigation measurements were processed every 30 minutes with a 2-n. mi. Mars-radius error. Table V is included to illustrate the possible advantages of using VTA guidance as opposed to using FTA guidance and to compare the effect on total ΔV when making one or two midcourse velocity corrections for either of these guidance types. The target point for each type of spacecraft guidance is the periapsis of the flyby hyperbola. In FTA guidance, a velocity correction is computed such that target position-vector deviations are nulled; the VTA technique (referred to as radius-of-periapsis guidance in ref. 4) allows the down-range position error at the target to be free while minimizing the magnitude of the calculated correction.

The choice of the timing of the corrections presented was based upon the comparison of the rms estimate of ΔV computed from equation (C8) and the rms uncertainty in the estimate ΔV_ϵ calculated from the square root of the trace of equation (C10). This procedure, discussed in reference 5, is based on the assumption that a guidance maneuver will be commanded only after a certain amount of confidence in the trajectory estimate has been obtained. This assumption implies that ΔV_ϵ should be smaller than ΔV, and the criterion chosen for this study was that $\Delta V_\epsilon / \Delta V \leq 0.5$. The philosophy of this choice of correction time will be discussed in more detail in the following section.

The procedure for computing the radius-of-periapsis dispersion which results from a guidance maneuver is presented in appendix E. The significance of this particular dispersion is that it is a measure of the "safe" planet periapsis passage of the spacecraft on the flyby hyperbola.

To compare FTA and VTA guidance for the spacecraft, consider table V(a). Assume that a single FTA correction is applied 0.86 hour before periapsis, then the required ΔV is 135 fps, with a resulting radius-of-periapsis dispersion of 1.48 n. mi.; a single VTA correction at the same time requires a ΔV of 117 fps, with a corresponding 1.42-n. mi. radius-of-periapsis dispersion. The reduction in ΔV of 18 fps is obtained at the expense of an increase in down-range position error of 35 n. mi. This increase in down-range error is not significant, however, since this component of position error can be mapped into a passage-of-periapsis timing error of a few seconds.

Again, consider table V(a) to compare the effect on total ΔV of making either one or two velocity corrections to achieve a specified radius-of-periapsis dispersion. Assume that a dispersion of 1.4 n. mi. is desired. A single FTA correction to produce this target dispersion requires a ΔV of 135 fps; if two corrections are applied, however, the same dispersion results for a total ΔV of 17 fps. Using two corrections also enables the target dispersion to be further reduced to 1.2 n. mi. for a total ΔV of 25 fps (FTA) and for a total ΔV of 23 fps (VTA).

The preceding discussion involves data that were computed using initial uncertainty and dispersion matrices generated from only Earth-based radar tracking during the Earth-to-Mars portion of the mission. A comparison of tables V(a) and V(b) illustrates the effect on the spacecraft midcourse velocity corrections in the Mars SOI of adding some onboard observations to the measurement schedule during the trans-Mars mission phase. The ΔV values in table V(b) are reduced, primarily because $E(t_0)$ generated from a combination of Earth-based radar and onboard tracking is much smaller than $E(t_0)$ generated from only Earth-based tracking. The initial dispersion matrix $X(t_0)$ is approximately the same for both types of tracking.

The preceding discussion for tables V(a) and V(b) (short-long trajectory) applies equally well to tables V(c) and V(d) (long-short trajectory).

Probe. - Figure 5 presents a comparison of the rms estimate of ΔV, the uncertainty in the estimate ΔV_ϵ, and the probe entry flight-path-angle dispersion $\Delta\gamma$, when

biased sextant-navigation measurements are processed at 30-minute intervals with a 2-n. mi. Mars-radius uncertainty. Figures 5(a) and 5(b) are plots for the short-long trajectory and the two sets of initial covariance matrices, while figures 5(c) and 5(d) are similar plots for the long-short trajectory. These plots illustrate the philosophy which might be used to select the time of a single velocity correction to achieve a specified target $\Delta\gamma$ dispersion while satisfying the criterion that $\Delta V_\epsilon/\Delta V \leq 0.5$.

Consider figure 5(a) and assume that an entry flight-path-angle dispersion of 0.16° is desired. A single correction 5 hours prior to the arrival at the nominal entry altitude will produce a $\Delta\gamma$ dispersion of 0.16° for a ΔV of 20 fps. The uncertainty in the velocity estimate at this point is 2 fps, so that $\Delta V_\epsilon/\Delta V = 0.1$ and the selection criterion is satisfied. Now consider figure 5(b) and assume a required $\Delta\gamma$ dispersion at entry of 0.155°. This dispersion can be achieved as early as 5 hours prior to entry, and the $\Delta\gamma$ plot is flat from that time on. Therefore, to keep the ΔV as small as possible, the earliest correction time is selected (i.e., 5 hours before entry). The rms ΔV is 3 fps, but ΔV_ϵ is 2 fps, so that $\Delta V_\epsilon/\Delta V = 0.67$ and the selection criterion is not satisfied. Similar discussion would apply to figures 5(c) and 5(d).

A representative set of probe guidance data is summarized in table VI. For these data, biased sextant-navigation measurements were processed at 30-minute intervals, assuming a 2-n. mi. Mars-radius uncertainty. The target of the FTA guidance technique is the probe vacuum periapsis, and this technique attempts to null the position-vector deviations at that point. The target of the VTA guidance technique is the nominal entry altitude, which allows the down-range position error to be free while nulling the entry flight-path-angle deviation. The procedures for calculating the probe radius-of-vacuum-periapsis dispersion and the entry flight-path-angle dispersion are outlined in appendix E. The $\Delta\gamma$ dispersions presented in table VI are computed for fixed radius (e.g., at the nominal entry altitude). The initial uncertainty and dispersion matrices for the probe were computed from the $E(t_0)$ and $X(t_0)$ of the spacecraft at the time of separation and were properly degraded as a result of the separation maneuver.

The data in table VI indicate that there is very little apparent difference between the FTA and VTA guidance for the probe. This might be expected to be the case if equation (D16) is compared to equation (D31). Equation (D16) presents the submatrices $G_1(t)$ and $G_2(t)$ of the guidance matrix $G(t)$ for FTA guidance; equation (D31) represents these submatrices for VTA guidance nulling $\Delta\gamma$ at the target. The submatrix $G_2(t)$ is the same for both guidance schemes, and $G_1(t)$ for the VTA guidance reduces to $G_1(t)$ for FTA guidance if

$$-\frac{\phi_{12}^{-1}\underline{v}_T\underline{Z}_2^T\left(\phi_{21}-\phi_{22}\phi_{12}^{-1}\phi_{11}\right)}{\left(\underline{Z}_1^T+\underline{Z}_2^T\phi_{22}\phi_{12}^{-1}\right)\underline{v}_T} \ll \phi_{12}^{-1}\phi_{11}$$

The interpretation of the data presented in table VI follows the same pattern as the interpretation of the spacecraft guidance data in table V. For example, consider table VI(a). A single FTA correction executed 0.83 hour before entry requires a ΔV of 111 fps with a corresponding $\Delta\gamma$ of 0.18°; if two corrections are applied, with the second correction applied 0.83 hour before entry, the total ΔV is 42 fps with a $\Delta\gamma$ of 0.16°. Again, the use of two corrections has produced a significant saving in ΔV. If VTA guidance is used for these same two corrections, the total ΔV is 44 fps with a $\Delta\gamma$ of 0.15°. The difference to be noted is that while the total ΔV is approximately the same, the $\Delta\gamma$ error is better controlled with VTA guidance, whereas the radius-of-vacuum-periapsis error is better controlled with FTA guidance. This is to be expected because of the nature of the two guidance laws being compared. The radius-of-vacuum-periapsis dispersion is a measure of the entry corridor, and by multiplying that number by some appropriate "safety" factor, the corridor width attainable by the guidance system can be computed. Normally, this safety factor is 6, so that for the cases just cited, the corridor widths would be 8.64 n. mi. and 9.18 n. mi., respectively.

Tables VI(b) and VI(d) present only single-correction results because two corrections to the probe trajectory were not necessary in these cases. These data resulted from the smaller initial probe uncertainty covariance matrix used. The discussion of the data in table VI(c) would be similar to that presented for table VI(a).

CONCLUDING REMARKS

The navigation and guidance analysis of a Mars probe launched from a manned flyby spacecraft has been presented. The study was initiated with the probe and spacecraft separation at the Mars sphere of influence and was terminated with the probe arrival at a specified entry altitude and with the spacecraft arrival at Mars periapsis. The results of the study indicate that spacecraft radius-of-periapsis dispersions between 1 and 6 n. mi. can be obtained for a total velocity between 10 and 150 fps. The probe entry flight-path-angle dispersions varied from 0.13° to 0.21° (corresponding to an entry corridor of 10 n. mi.) for approximately the same range in velocity. These results are very dependent on the initial spacecraft errors at the time of separation and on the system model errors assumed when processing navigation data.

Manned Spacecraft Center
National Aeronautics and Space Administration
Houston, Texas, January 10, 1968
981-30-89-00-72

TABLE I. - SPACECRAFT UNCERTAINTY AND DISPERSION COVARIANCE MATRICES AT MARS SPHERE OF INFLUENCE IN MARS EQUATORIAL COORDINATE SYSTEM, ft, fps

(a) Generated from Earth-based radar tracking only

$$E(t_0) = \begin{bmatrix} +0.10795743E+11 & +0.65967692E+09 & +0.33814298E+11 & +0.18949483E+04 & -0.37702034E+03 & +0.10354719E+04 \\ & +0.18766645E+10 & +0.70484404E+10 & -0.53478838E+03 & +0.10425965E+04 & +0.42295007E+03 \\ & & +0.11982285E+12 & +0.39853662E+04 & +0.16151761E+04 & +0.43253749E+04 \\ & & & +0.17066236E-02 & -0.45197054E-03 & +0.26474908E-03 \\ & (\text{Symmetric}) & & & +0.16697713E-02 & +0.20050646E-03 \\ & & & & & +0.21117166E-02 \end{bmatrix}$$

$$X(t_0) = \begin{bmatrix} +0.73819030E+12 & +0.15401839E+12 & -0.93253504E+11 & -0.86159568E+07 & -0.18965936E+07 & +0.15584321E+07 \\ & +0.17476617E+12 & -0.70977560E+11 & -0.18317749E+07 & -0.20811097E+07 & +0.93663495E+06 \\ & & +0.28377198E+12 & +0.15426505E+07 & +0.95201726E+06 & -0.18607330E+07 \\ & & & +0.10291022E+03 & +0.22766192E+02 & -0.18675098E+02 \\ & (\text{Symmetric}) & & & +0.25288863E+02 & -0.11509438E+02 \\ & & & & & +0.22327910E+02 \end{bmatrix}$$

TABLE I.- SPACECRAFT UNCERTAINTY AND DISPERSION COVARIANCE MATRICES AT MARS SPHERE OF INFLUENCE IN MARS EQUATORIAL COORDINATE SYSTEM, ft, fps - Concluded

(b) Generated from Earth-based radar and onboard tracking

$$E(t_0) = \begin{bmatrix} +0.59298541E+09 & -0.49410256E+09 & +0.34391141E+09 & +0.33825529E+03 & -0.31423879E+03 & -0.47339011E+02 \\ & +0.64494082E+09 & +0.16991217E+09 & -0.28329428E+03 & +0.43679336E+03 & +0.61234597E+02 \\ & & +0.15493640E+10 & -0.17214476E+01 & +0.65811396E+02 & +0.15218244E+03 \\ & & & +0.16175887E+00 & +0.25352728E-01 & -0.18663014E-01 \\ & (\text{Symmetric}) & & & +0.37405348E-01 & -0.11504193E-01 \\ & & & & & +0.62743453E-01 \end{bmatrix}$$

$$X(t_0) = \begin{bmatrix} +0.73238785E+12 & +0.15312751E+12 & -0.11271050E+12 & -0.11453944E+08 & -0.23871738E+07 & +0.17817307E+07 \\ & +0.17436720E+12 & -0.74533639E+11 & -0.24086431E+07 & -0.26909167E+07 & +0.11632760E+07 \\ & & +0.21538386E+12 & +0.17784900E+07 & +0.11575928E+07 & -0.31164389E+07 \\ & & & +0.17944820E+03 & +0.37444451E+02 & -0.28045894E+02 \\ & (\text{Symmetric}) & & & +0.41732681E+02 & -0.18035724E+02 \\ & & & & & +0.51504544E+02 \end{bmatrix}$$

TABLE II. - NOMINAL ROOT-MEAN-SQUARE ERROR VALUES, 1σ

Errors in making velocity correction:	
Magnitude, percent	1
Direction, deg	1
Cutoff, fps	0.5
Observation noise:	
Instrument error, σ_I, arc sec	5
Radius uncertainty/planet radius, c	0.01/0.001
Instrument bias, σ_B, arc sec	60

TABLE III. - COMPARISON OF SHORT-LONG (SEPTEMBER 20, 1975, LAUNCH) AND LONG-SHORT (APRIL 17, 1976, LAUNCH) MARS FLYBY TRAJECTORY CHARACTERISTICS

Trajectory designation	Short-long	Long-short
Julian date of launch from Earth	2 442 675.0	2 442 885.0
Earth injection-velocity magnitude, fps	15 150	14 050
Declination of Earth departure asymptote, deg	33.31	-30.24
Outbound-trip time, days	133.29	582.21
Return-trip time, days	538.64	98.37
Time in Mars SOI, hr	37.74	29.92
Periapsis altitude at Mars, n. mi.	106.09	112.67
General location of periapsis at Mars	Northern hemisphere	Southern hemisphere
Inclination to Mars equator, deg	144.21	13.10
Lighting conditions	Periapsis-dark	Periapsis-light
Entry velocity at Earth, fps	47 900	51 300

TABLE IV.- INITIAL POSITION AND VELOCITY OF FLYBY SPACECRAFT AT MARS SPHERE OF INFLUENCE IN MARS EQUATORIAL COORDINATE SYSTEM FOR SHORT-LONG AND LONG-SHORT TRAJECTORIES, n. mi., fps

Short-long		
X	Y	Z
-0.30318650E+06	-0.57007078E+05	+0.52589475E+05
$\dot{X}$	$\dot{Y}$	$\dot{Z}$
+0.27000551E+05	+0.52456193E+04	-0.45743130E+04
Long-short		
X	Y	Z
+0.30693083E+06	+0.58836092E+05	-0.16437793E+05
$\dot{X}$	$\dot{Y}$	$\dot{Z}$
-0.34589177E+05	-0.63904358E+04	+0.17966413E+04

TABLE V.- SPACECRAFT ROOT-MEAN-SQUARE ΔV SUMMARY WITH BIASED SEXTANT-NAVIGATION MEASUREMENTS PROCESSED EVERY 30 MINUTES, ASSUMING A 2-NAUTICAL MILE MARS-RADIUS ERROR

(a) Short-long trajectory; $E(t_0)$, $X(t_0)$ generated using Earth-based radar tracking only

Guidance scheme	Root-mean-square ΔV_1, fps	Time of ΔV_1 measured from Mars periapsis, hr	Root-mean-square ΔV_2, fps	Time of ΔV_2 measured from Mars periapsis, hr	Total ΔV, fps	Radius-of-periapsis dispersion, n. mi.
Fixed time of arrival	10.46	11.36	-	-	10.46	5.38
	15.15	7.86	-	-	15.15	3.42
	41.39	2.86	-	-	41.39	1.86
	135.00	.86	-	-	135.00	1.48
	10.46	11.36	1.62	6.86	12.08	3.41
	10.46	11.36	5.37	2.36	15.83	1.80
	10.46	11.36	6.85	1.86	17.31	1.49
	10.46	11.36	14.80	.86	25.26	1.25
Variable time of arrival	9.31	11.36	-	-	9.31	5.44
	13.47	7.86	-	-	13.47	3.45
	36.57	2.86	-	-	36.57	1.83
	117.65	.86	-	-	117.65	1.42
	9.31	11.36	1.55	6.86	10.86	3.48
	9.31	11.36	5.16	2.36	14.47	1.83
	9.31	11.36	6.58	1.86	15.89	1.51
	9.31	11.36	14.08	.86	23.39	1.26

TABLE V.- SPACECRAFT ROOT-MEAN-SQUARE ΔV SUMMARY WITH BIASED SEXTANT-NAVIGATION MEASUREMENTS PROCESSED EVERY 30 MINUTES, ASSUMING A 2-NAUTICAL MILE MARS-RADIUS ERROR - Continued

(b) Short-long trajectory; $E(t_0)$, $X(t_0)$ generated using Earth-based radar and onboard tracking

Guidance scheme	Root-mean-square ΔV_1, fps	Time of ΔV_1 measured from Mars periapsis, hr	Root-mean-square ΔV_2, fps	Time of ΔV_2 measured from Mars periapsis, hr	Total ΔV, fps	Radius-of-periapsis dispersion, n. mi.
Fixed time of arrival	5.82	11.36	-	-	5.82	3.92
	8.46	7.86	-	-	8.46	2.83
	23.49	2.86	-	-	23.49	1.63
	79.25	.86	-	-	79.25	1.28
	5.82	11.36	1.05	6.86	6.87	3.00
	5.82	11.36	3.69	2.36	9.51	1.68
	5.82	11.36	4.74	1.86	10.56	1.42
	5.82	11.36	10.28	.86	16.10	1.21
Variable time of arrival	3.51	11.36	-	-	3.51	4.23
	5.12	7.86	-	-	5.12	3.02
	13.98	2.86	-	-	13.98	1.63
	45.05	.86	-	-	45.05	1.21
	3.51	11.36	1.06	6.86	4.57	3.28
	3.51	11.36	3.86	2.36	7.37	1.84
	3.51	11.36	4.96	1.86	8.47	1.53
	3.51	11.36	10.70	.86	14.21	1.28

TABLE V.- SPACECRAFT ROOT-MEAN-SQUARE ΔV SUMMARY WITH BIASED SEXTANT-NAVIGATION MEASUREMENTS PROCESSED EVERY 30 MINUTES, ASSUMING A 2-NAUTICAL MILE MARS-RADIUS ERROR - Continued

(c) Long-short trajectory; $E(t_0)$, $X(t_0)$ generated using Earth-based radar tracking only

Guidance scheme	Root-mean-square ΔV_1, fps	Time of ΔV_1 measured from Mars periapsis, hr	Root-mean-square ΔV_2, fps	Time of ΔV_2 measured from Mars periapsis, hr	Total ΔV, fps	Radius-of-periapsis dispersion, n. mi.
Fixed time of arrival	19.73	7.46	-	-	19.73	3.88
	27.00	5.46	-	-	27.00	2.59
	49.85	2.96	-	-	49.85	2.11
	153.84	.96	-	-	153.84	1.58
	19.73	7.46	1.73	4.96	21.46	2.61
	19.73	7.46	3.37	2.96	23.10	2.12
	19.73	7.46	5.30	1.96	25.03	1.51
	19.73	7.46	22.86	.46	42.59	1.21
Variable time of arrival	15.18	7.46	-	-	15.18	3.87
	20.75	5.46	-	-	20.75	2.53
	38.13	2.96	-	-	38.13	2.01
	115.76	.96	-	-	115.76	1.41
	15.18	7.46	1.60	4.96	16.78	2.61
	15.18	7.46	3.18	2.96	18.36	2.12
	15.18	7.46	4.98	1.96	20.16	1.50
	15.18	7.46	21.63	.46	36.81	1.20

TABLE V.- SPACECRAFT ROOT-MEAN-SQUARE ΔV SUMMARY WITH BIASED SEXTANT-NAVIGATION MEASUREMENTS PROCESSED EVERY 30 MINUTES, ASSUMING A 2-NAUTICAL MILE MARS-RADIUS ERROR - Concluded

(d) Long-short trajectory; $E(t_0)$, $X(t_0)$ generated using Earth-based radar and onboard tracking

Guidance scheme	Root-mean-square ΔV_1, fps	Time of ΔV_1 measured from Mars periapsis, hr	Root-mean-square ΔV_2, fps	Time of ΔV_2 measured from Mars periapsis, hr	Total ΔV, fps	Radius-of-periapsis dispersion, n. mi.
Fixed time of arrival	14.83	7.46	-	-	14.83	3.13
	20.32	5.46	-	-	20.32	2.27
	37.65	2.96	-	-	37.65	1.87
	117.58	.96	-	-	117.58	1.38
	14.83	7.46	1.18	4.96	16.01	2.40
	14.83	7.46	2.40	2.96	17.23	1.97
	14.83	7.46	3.84	1.96	18.67	1.45
	14.83	7.46	16.83	.46	31.66	1.17
Variable time of arrival	8.40	7.46	-	-	8.40	3.28
	11.50	5.46	-	-	11.50	2.34
	21.16	2.96	-	-	21.16	1.81
	64.39	.96	-	-	64.39	1.20
	8.40	7.46	1.11	4.96	9.51	2.58
	8.40	7.46	2.34	2.96	10.74	2.13
	8.40	7.46	3.75	1.96	12.15	1.55
	8.40	7.46	16.63	.46	25.03	1.23

TABLE VI. - PROBE ROOT-MEAN-SQUARE ΔV SUMMARY WITH BIASED SEXTANT-NAVIGATION MEASUREMENTS PROCESSED EVERY 30 MINUTES, ASSUMING A 2-NAUTICAL MILE MARS-RADIUS ERROR

(a) Short-long trajectory; $E(t_0)$, $X(t_0)$ generated using Earth-based radar and onboard tracking.

Guidance scheme	Root-mean-square ΔV_1, fps	Time of ΔV_1 measured from entry, hr	Root-mean-square ΔV_2, fps	Time of ΔV_2 measured from entry, hr	Total ΔV, fps	Radius-of-vacuum-periapsis dispersion, n. mi.	Entry flight-path-angle dispersion, deg
Fixed time of arrival	7.18	13.33	-	-	7.18	11.41	0.21
	10.14	9.83	-	-	10.14	5.45	.17
	25.79	3.83	-	-	25.79	2.36	.16
	111.22	.83	-	-	111.22	1.56	.18
	7.18	13.33	3.34	8.83	10.52	5.19	.17
	7.18	13.33	8.05	3.83	15.23	2.38	.15
	7.18	13.33	35.29	.83	42.47	1.44	.16
	7.18	13.33	81.24	.33	88.42	1.40	.17
Variable time of arrival	7.20	13.33	-	-	7.20	11.41	0.21
	10.18	9.83	-	-	10.18	5.45	.17
	26.05	3.83	-	-	26.05	2.39	.15
	116.47	.83	-	-	116.47	2.19	.15
	7.20	13.33	3.35	8.83	10.55	5.20	.17
	7.20	13.33	8.14	3.83	15.34	2.39	.15
	7.20	13.33	37.18	.83	44.38	1.53	.15
	7.20	13.33	93.36	.33	100.56	1.82	.15

TABLE VI. - PROBE ROOT-MEAN-SQUARE ΔV SUMMARY WITH BIASED SEXTANT-NAVIGATION MEASUREMENTS PROCESSED EVERY 30 MINUTES, ASSUMING A 2-NAUTICAL MILE MARS-RADIUS ERROR - Continued

(b) Short-long trajectory; $E(t_0)$, $X(t_0)$ generated using Earth-based radar and onboard tracking

Guidance scheme	Root-mean-square ΔV, fps	Time of ΔV measured from entry, hr	Radius-of-vacuum-periapsis dispersion, n. mi.	Entry flight-path-angle dispersion, deg
Fixed	3.83	3.83	2.18	0.15
time	5.20	2.83	1.97	.15
of	8.01	1.83	1.69	.15
arrival	40.07	.33	1.24	.16
Variable	3.88	3.83	2.19	0.15
time	5.29	2.83	1.98	.15
of	8.24	1.83	1.70	.15
arrival	47.08	.33	1.37	.15

TABLE VI. - PROBE ROOT-MEAN-SQUARE ΔV SUMMARY WITH BIASED SEXTANT-NAVIGATION MEASUREMENTS PROCESSED EVERY 30 MINUTES, ASSUMING A 2-NAUTICAL MILE MARS-RADIUS ERROR - Continued

(c) Long-short trajectory; $E(t_0)$, $X(t_0)$ generated using Earth-based radar tracking only

Guidance scheme	Root-mean-square ΔV_1, fps	Time of ΔV_1 measured from entry, hr	Root-mean-square ΔV_2, fps	Time of ΔV_2 measured from entry, hr	Total ΔV, fps	Radius-of-vacuum-periapsis dispersion, n. mi.	Entry flight-path-angle dispersion, deg
Fixed time of arrival	9.77	9.87	-	-	9.77	7.25	0.19
	18.58	5.37	-	-	18.58	3.47	.14
	70.75	1.37	-	-	70.75	1.67	.13
	238.92	.37	-	-	238.92	1.43	.14
	9.77	9.87	5.13	5.37	14.90	3.56	.14
	9.77	9.87	11.91	2.37	21.68	2.06	.13
	9.77	9.87	20.36	1.37	30.13	1.45	.13
	9.77	9.87	69.12	.37	78.89	1.32	.13
Variable time of arrival	9.80	9.87	-	-	9.80	7.25	0.19
	18.68	5.37	-	-	18.68	3.48	.14
	72.22	1.37	-	-	72.22	1.72	.13
	256.53	.37	-	-	256.53	1.92	.13
	9.80	9.87	5.15	5.37	14.95	3.56	.14
	9.80	9.87	12.02	2.37	21.82	2.07	.13
	9.80	9.87	20.70	1.37	30.50	1.47	.13
	9.80	9.87	73.27	.37	83.07	1.46	.13

TABLE VI. - PROBE ROOT-MEAN-SQUARE ΔV SUMMARY WITH BIASED SEXTANT-NAVIGATION MEASUREMENTS PROCESSED EVERY 30 MINUTES, ASSUMING A 2-NAUTICAL MILE MARS-RADIUS ERROR - Concluded

(d) Long-short trajectory; $E(t_0)$, $X(t_0)$ generated using Earth-based radar and onboard tracking

Guidance scheme	Root-mean-square ΔV, fps	Time of ΔV measured from entry, hr	Radius-of-vacuum-periapsis dispersion, n. mi.	Entry flight-path-angle dispersion, deg
Fixed	6.01	2.37	1.87	0.13
time	10.39	1.37	1.47	.13
of	16.15	.87	1.34	.13
arrival	35.51	.37	1.22	.13
Variable	6.01	2.37	1.88	0.13
time	10.52	1.37	1.48	.13
of	16.46	.87	1.36	.13
arrival	37.23	.37	1.29	.12

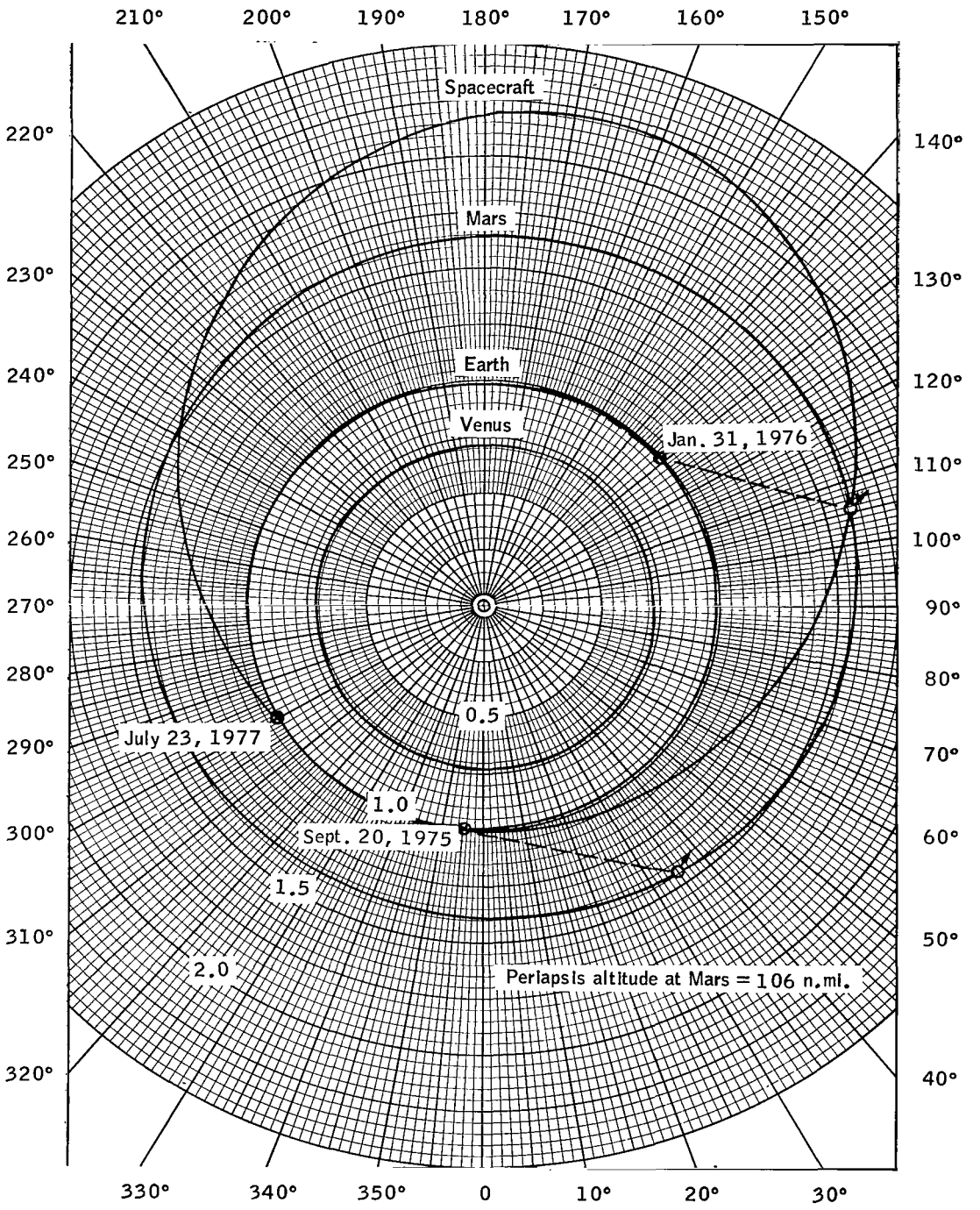

(a) Launch date — September 20, 1975 (short-long).

Figure 1. - Projection of free-return trajectories into the ecliptic plane.

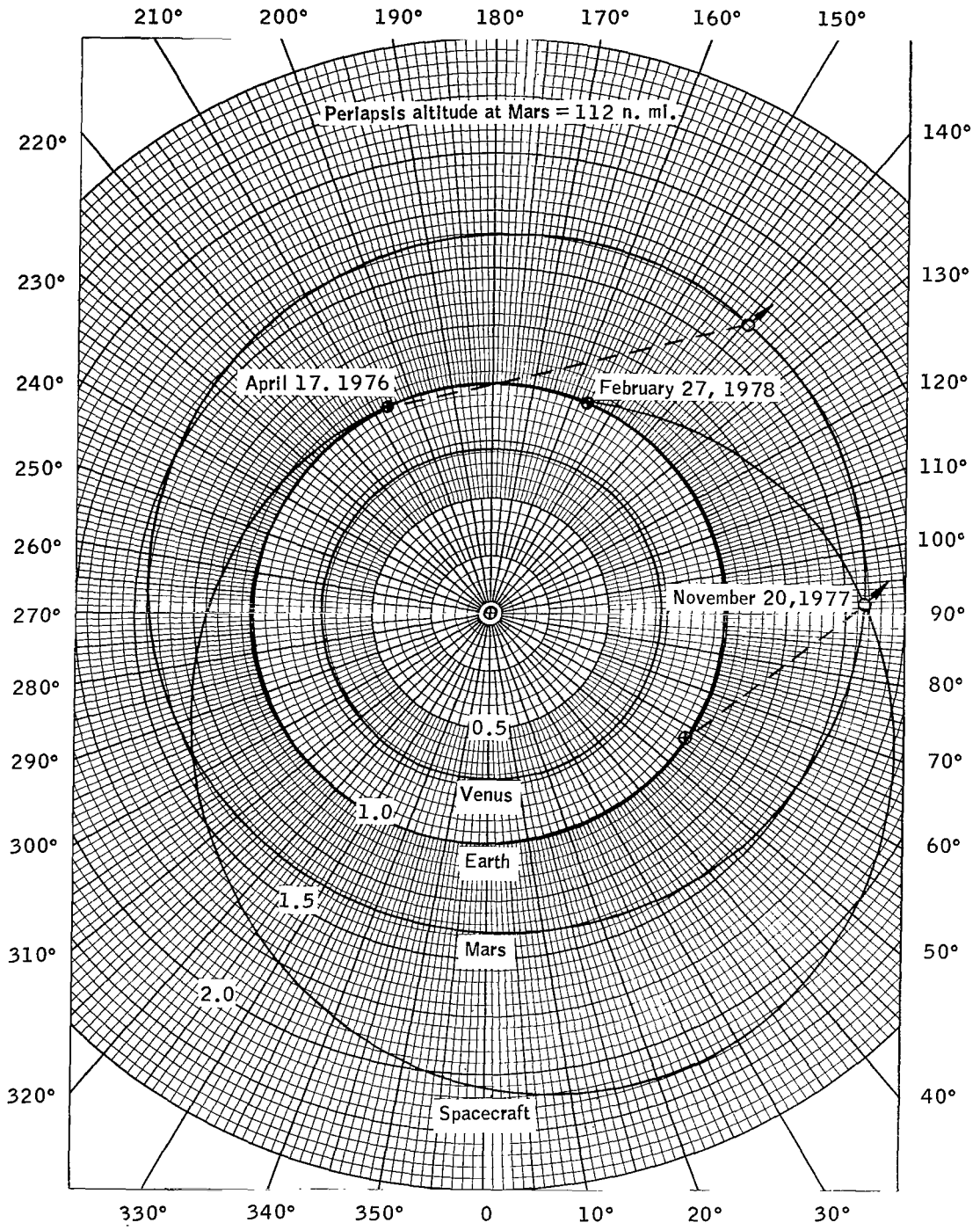

(b) Launch date — April 17, 1976 (long-short).

Figure 1. - Concluded.

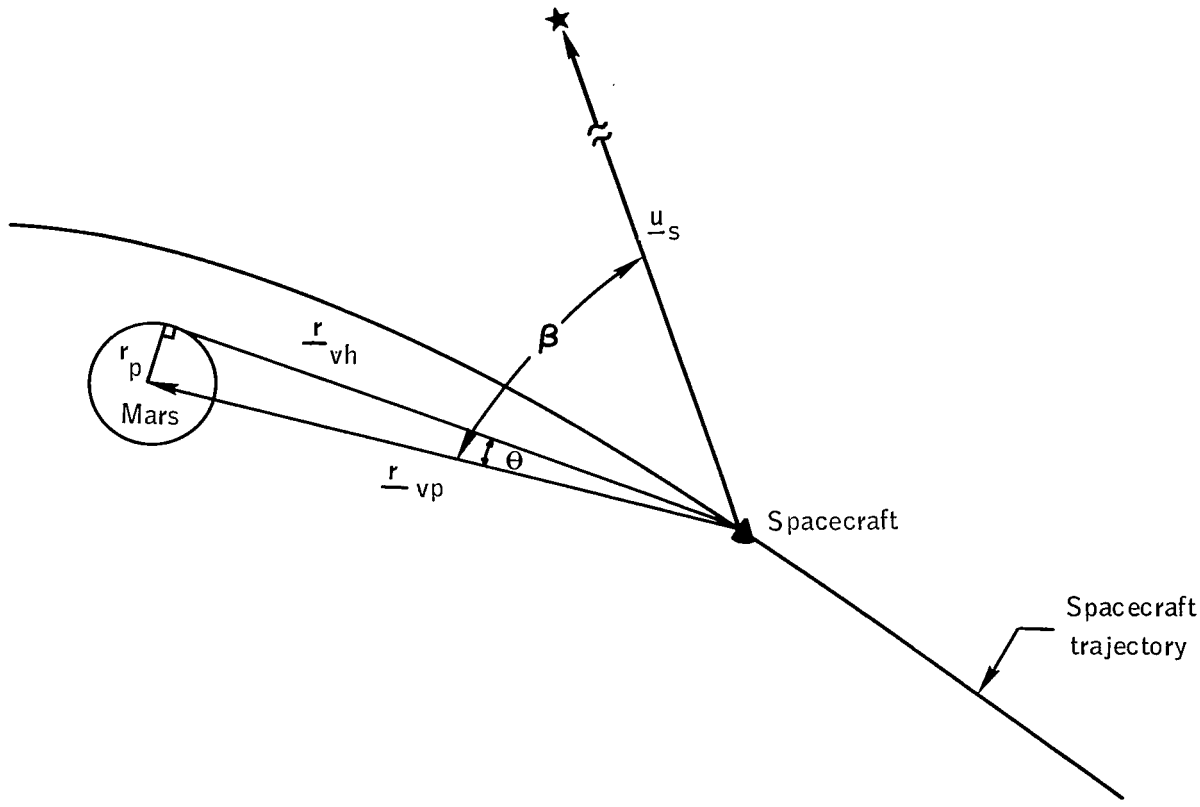

Figure 2.- Geometry of star-planet included-angle measurement.

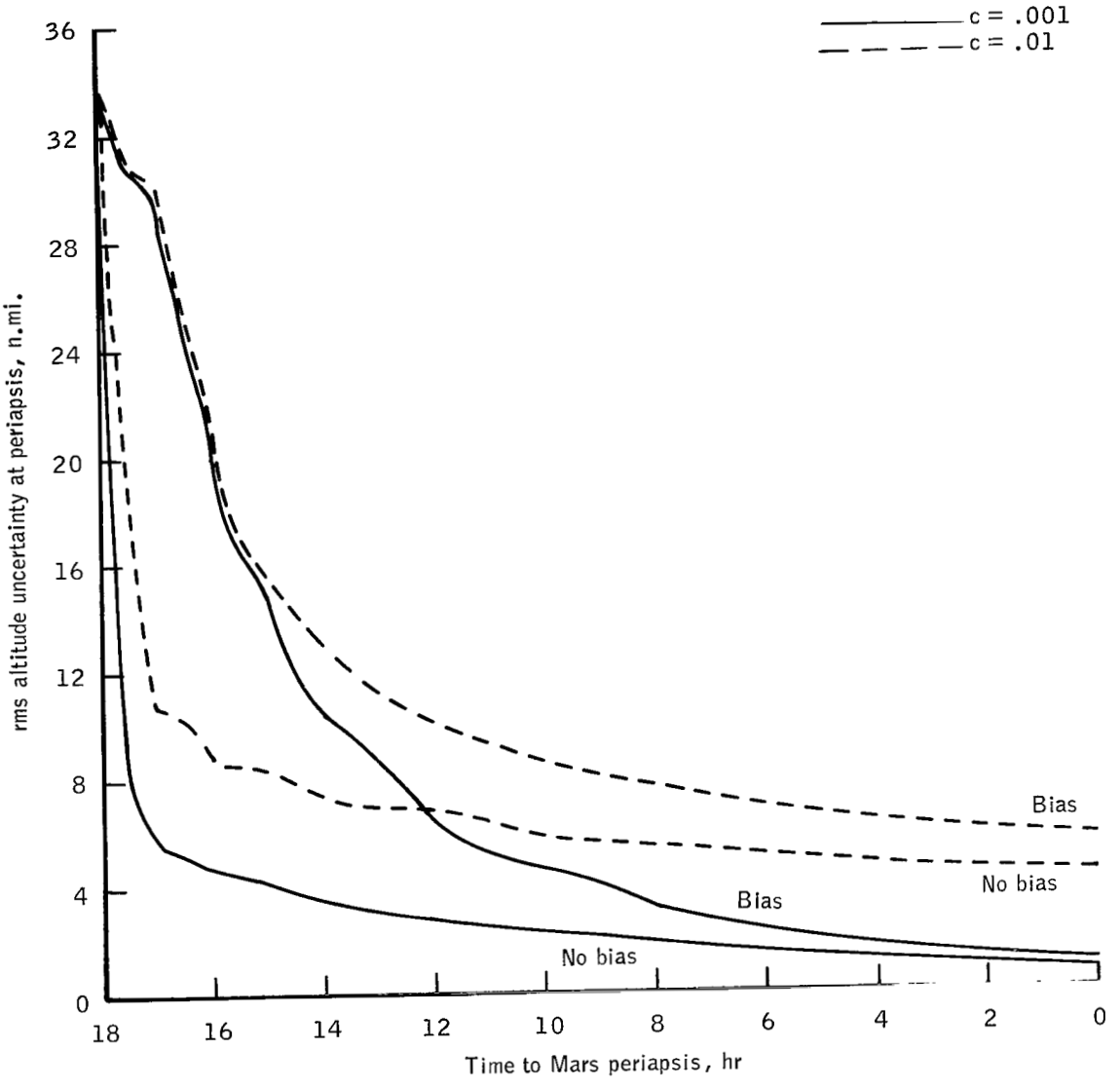

(a) Short-long trajectory; $E(t_0)$, $X(t_0)$ generated from Earth-based radar tracking only.

Figure 3. - Spacecraft rms periapsis-altitude uncertainties with sextant-navigation measurements processed every 30 minutes.

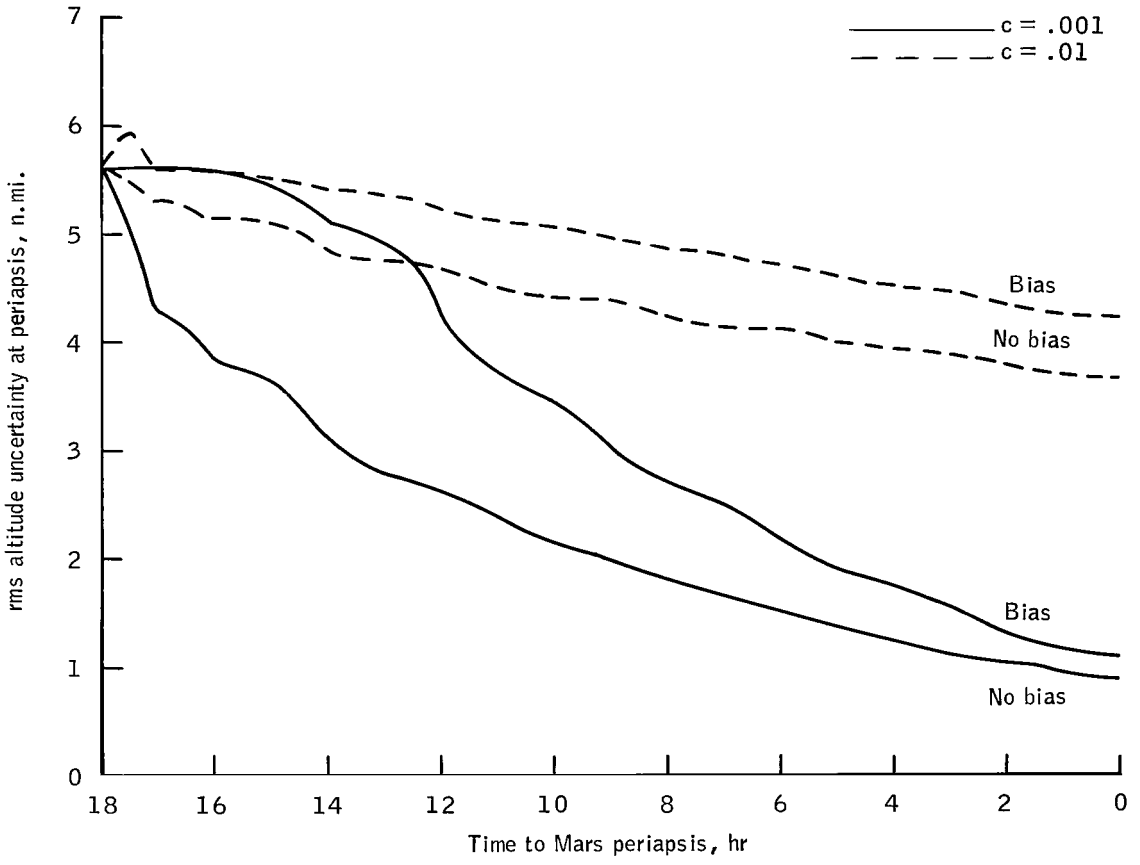

(b) Short-long trajectory; $E(t_0)$, $X(t_0)$ generated from Earth-based radar and onboard tracking.

Figure 3. - Continued.

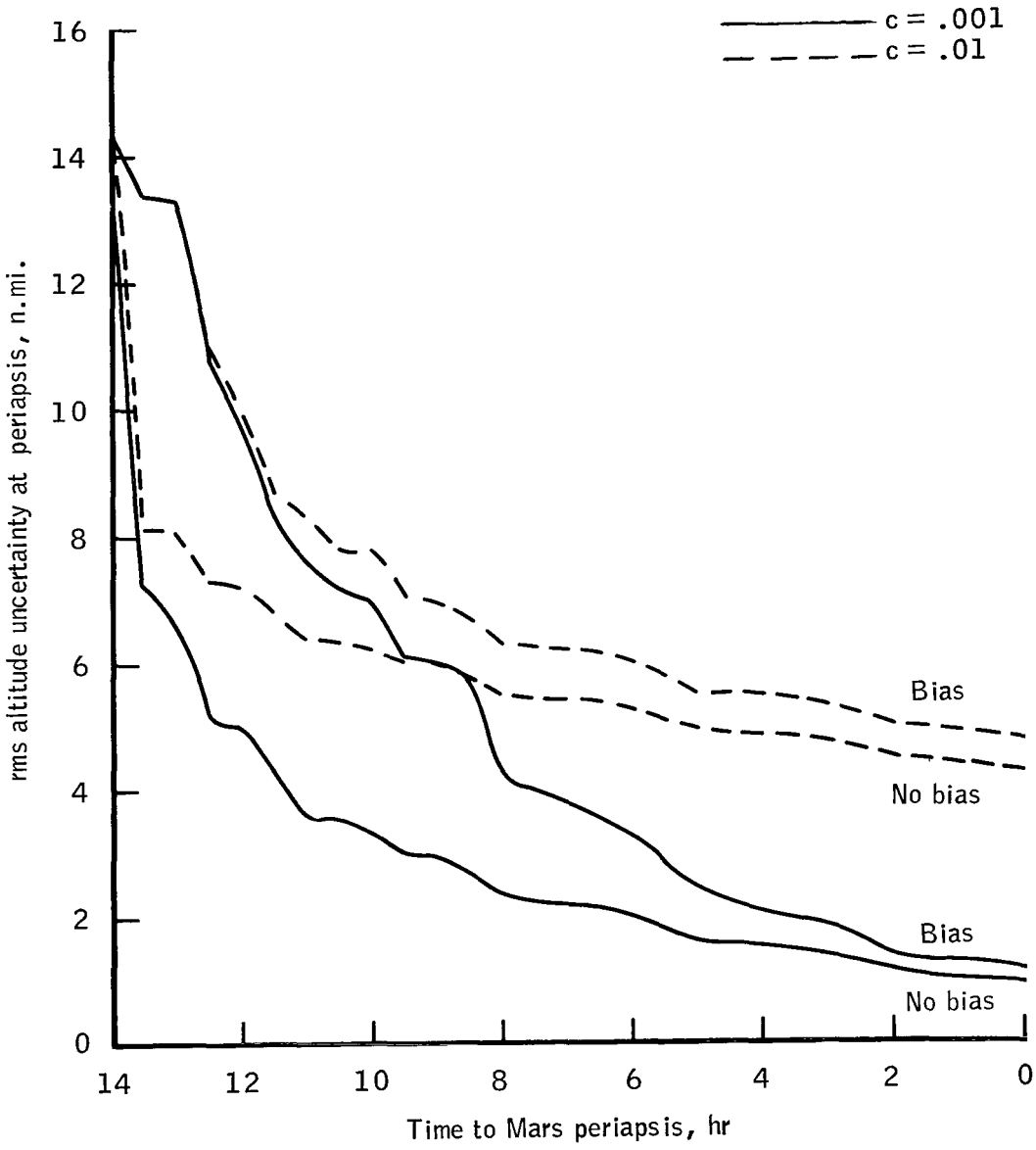

(c) Long-short trajectory; $E(t_0)$, $X(t_0)$ generated from Earth-based radar tracking only.

Figure 3. - Continued.

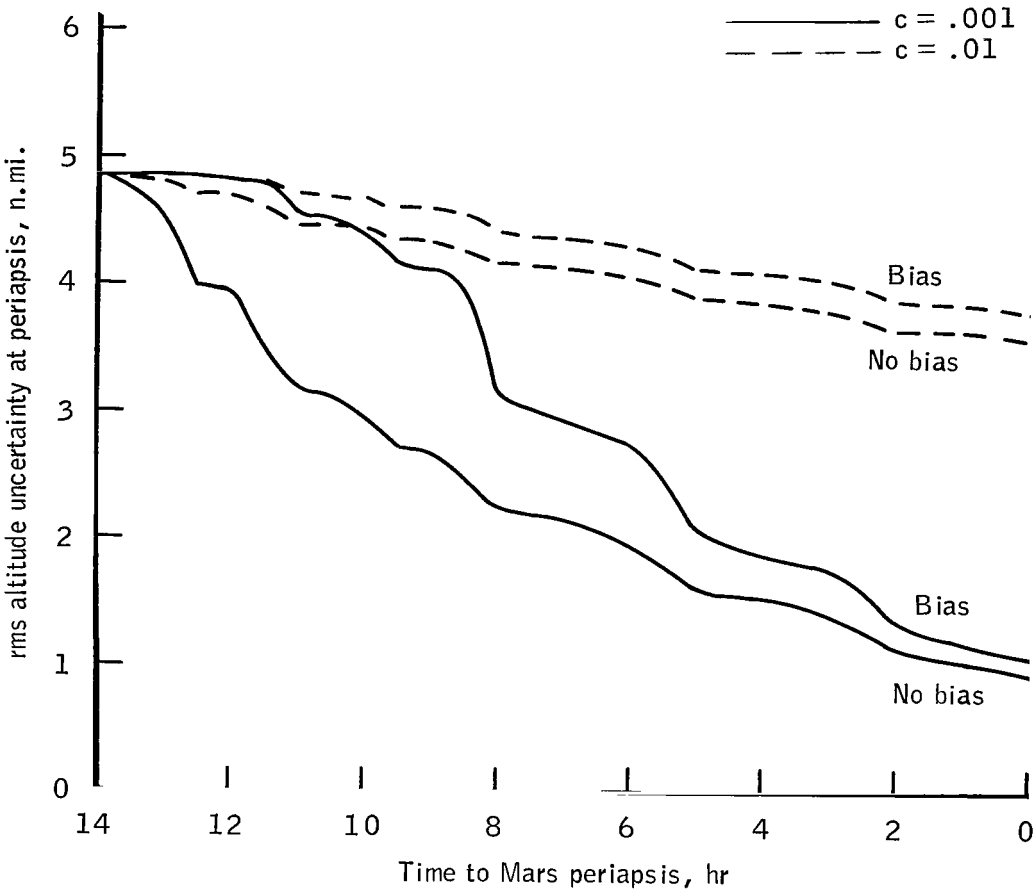

(d) Long-short trajectory; $E(t_0)$, $X(t_0)$ generated from Earth-based radar and onboard tracking.

Figure 3. - Concluded.

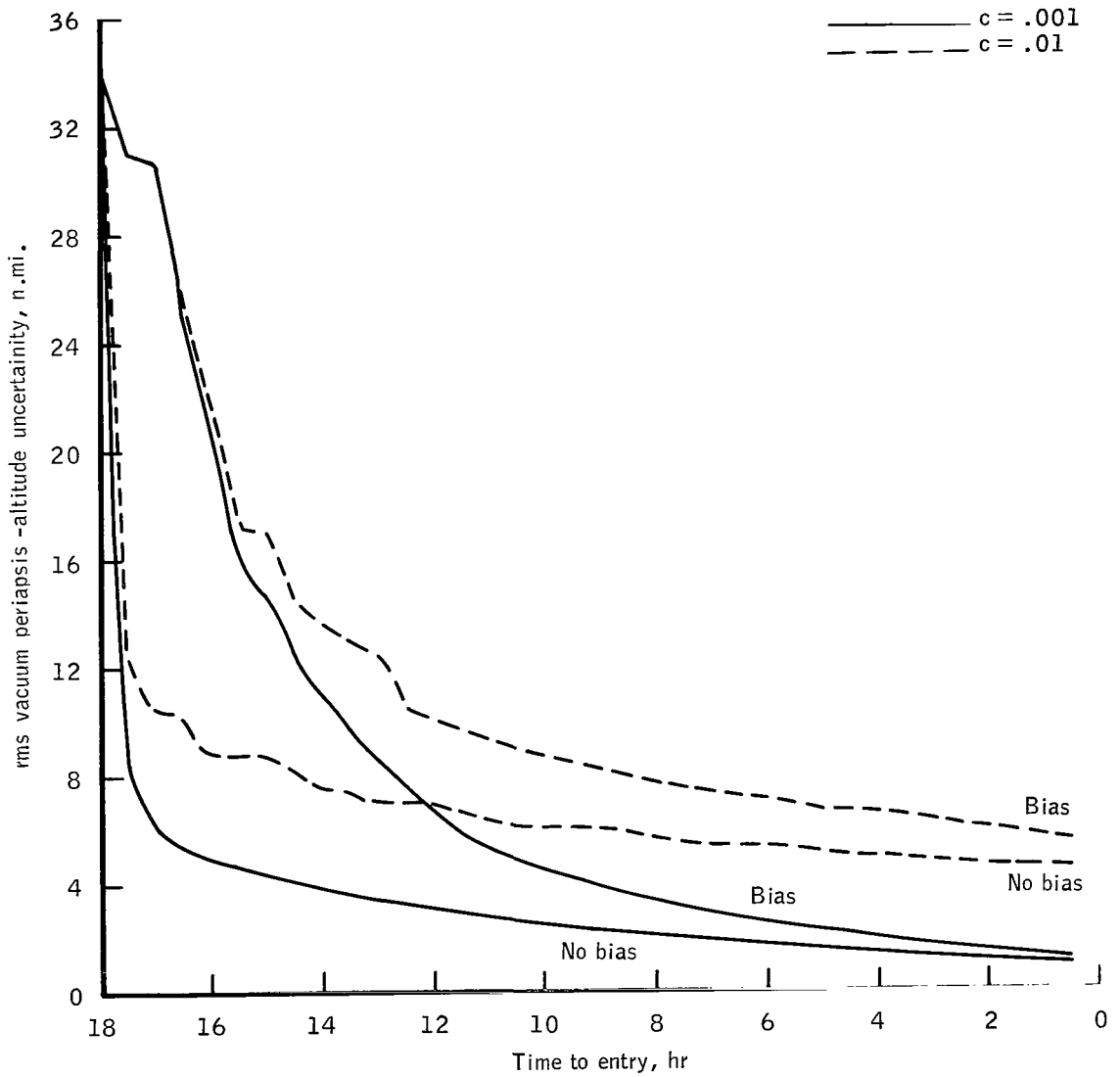

(a) Short-long trajectory; $E(t_0)$, $X(t_0)$ generated from Earth-based radar tracking only.

Figure 4. - Probe rms vacuum periapsis-altitude uncertainties with sextant-navigation measurements processed every 30 minutes.

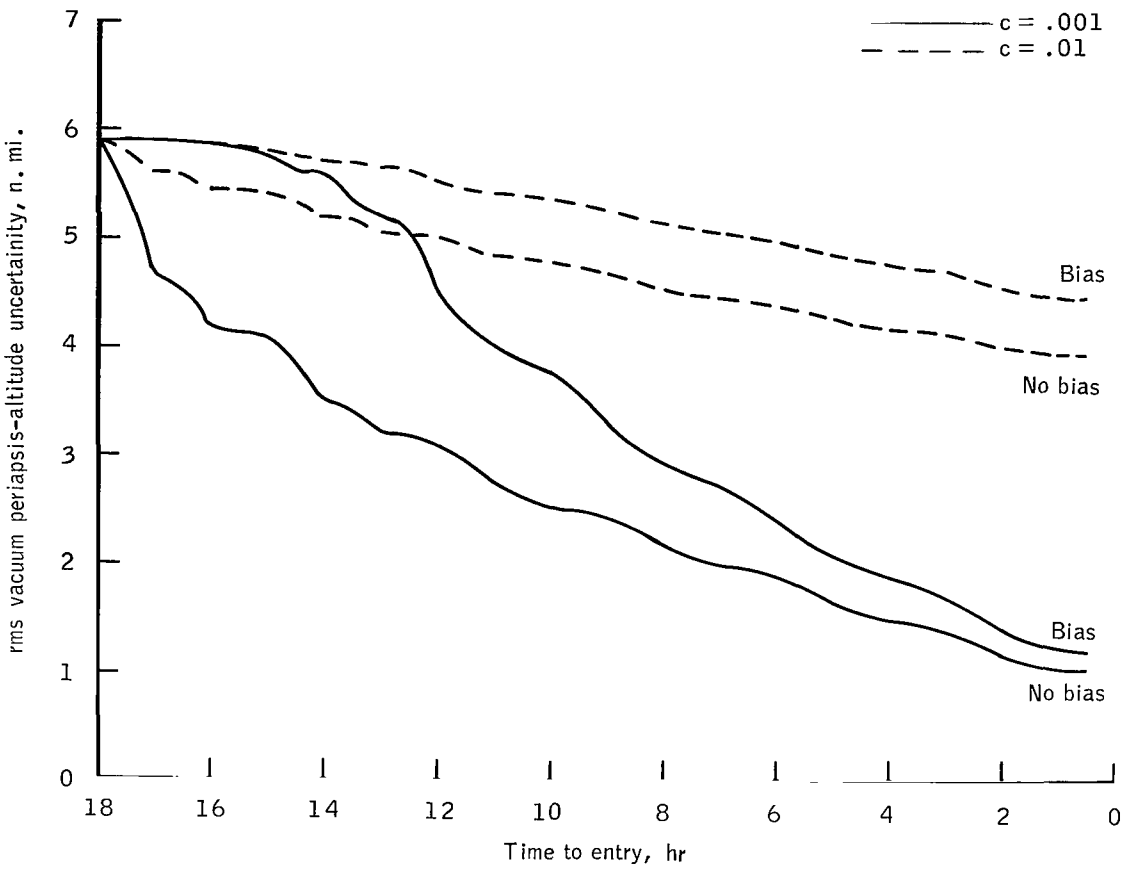

(b) Short-long trajectory; $E(t_0)$, $X(t_0)$ generated from Earth-based radar and onboard tracking.

Figure 4. - Continued.

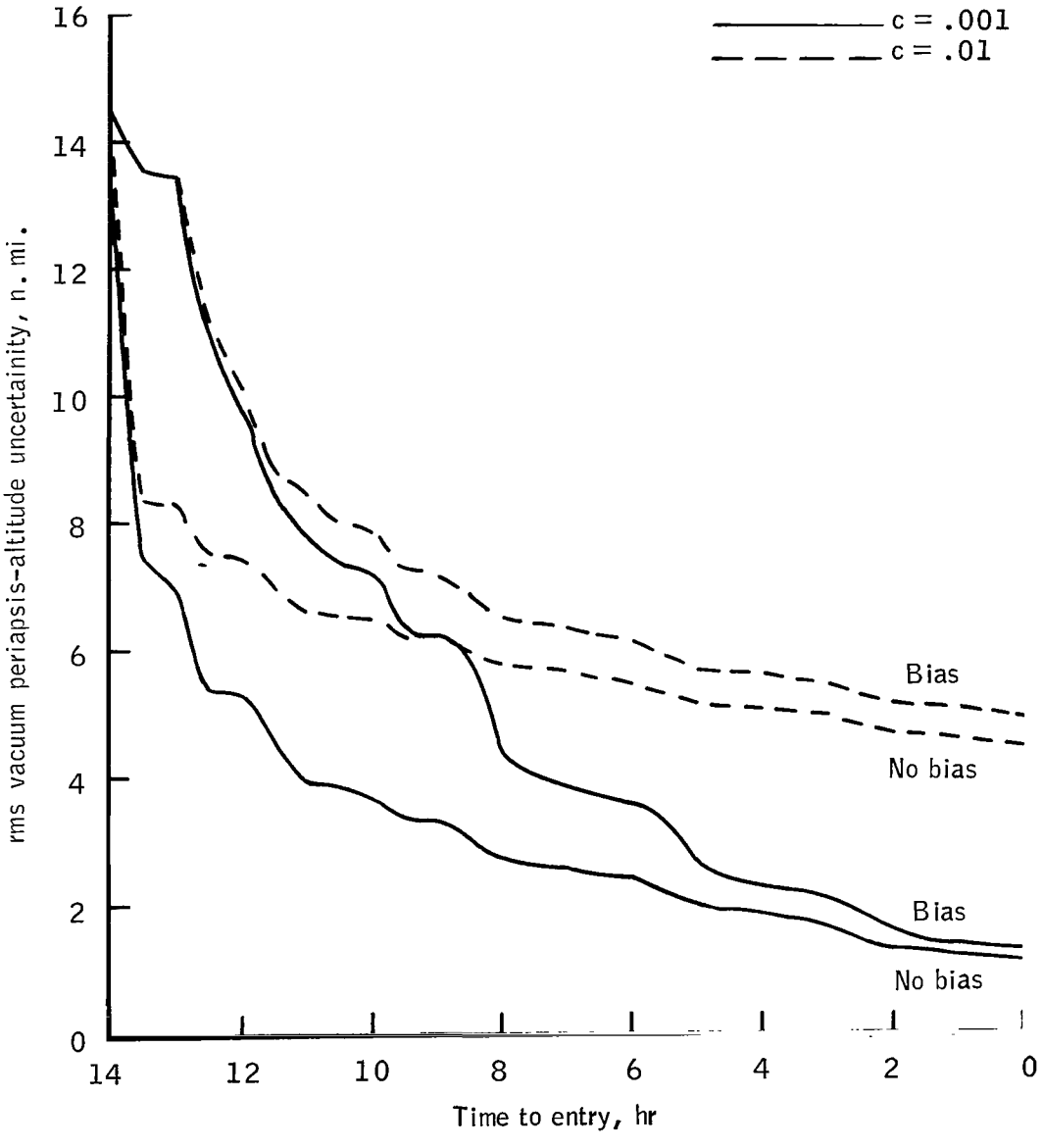

(c) Long-short trajectory; $E(t_0)$, $X(t_0)$ generated from Earth-based radar tracking only.

Figure 4. - Continued.

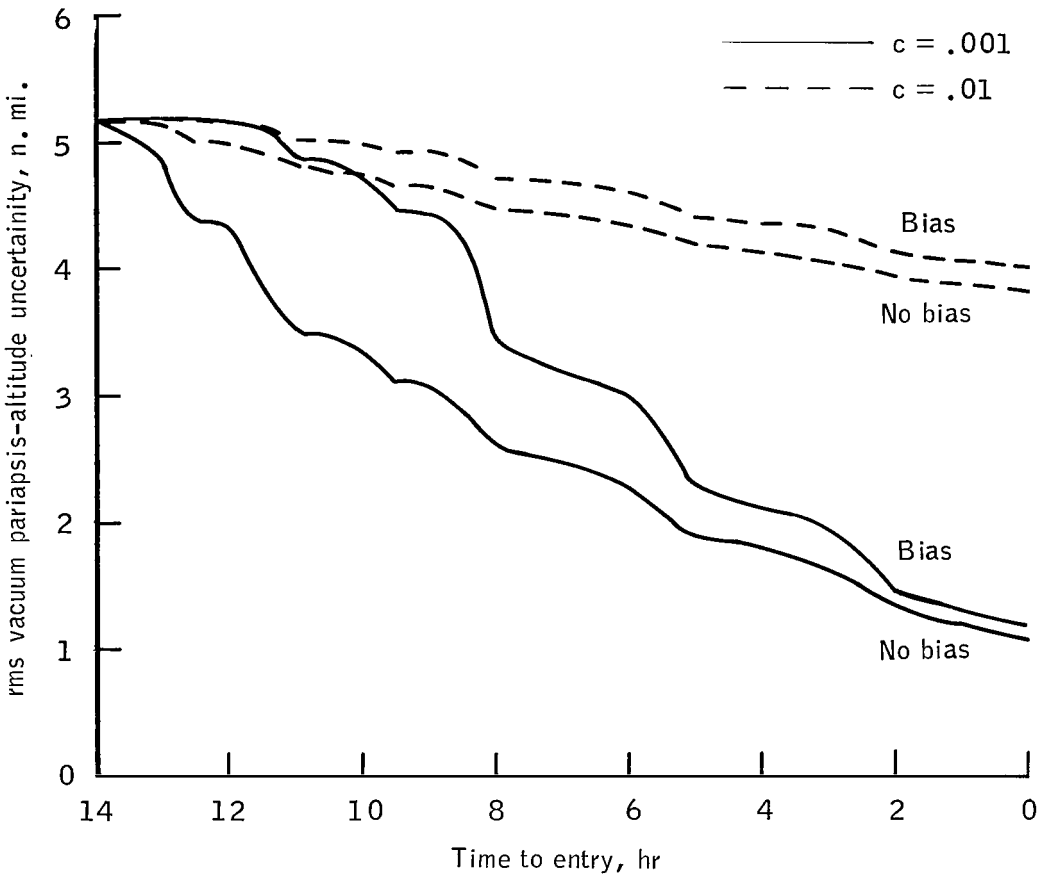

(d) Long-short trajectory; $E(t_0)$, $X(t_0)$ generated from Earth-based radar and onboard tracking.

Figure 4. - Concluded.

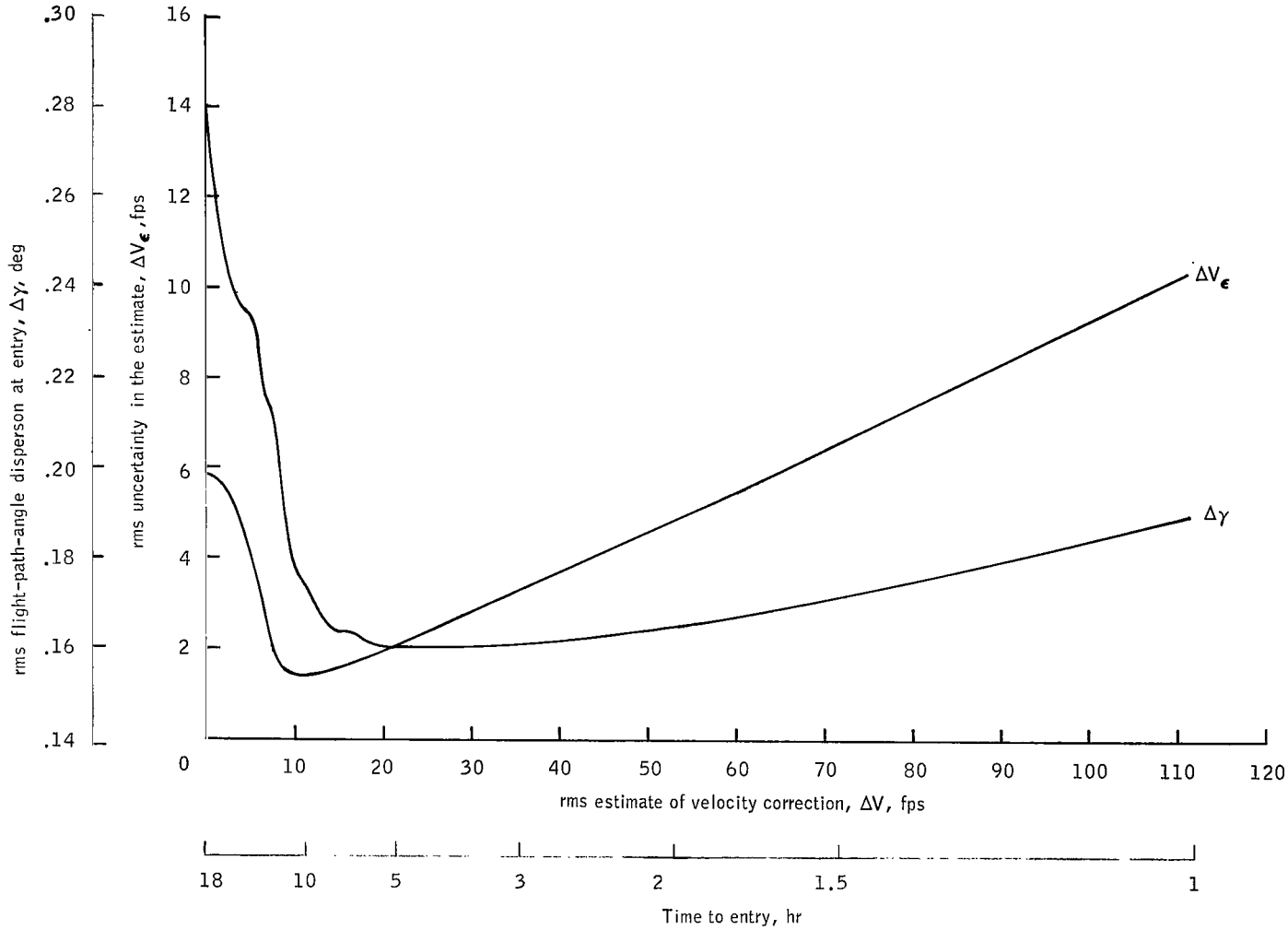

(a) Short-long trajectory; $\mathbf{E}(t_0)$, $\mathbf{X}(t_0)$ generated from Earth-based radar tracking only.

Figure 5. - Comparison of the rms estimate of velocity correction, the rms uncertainty in the estimate, and the resulting probe entry flight-path-angle dispersion.

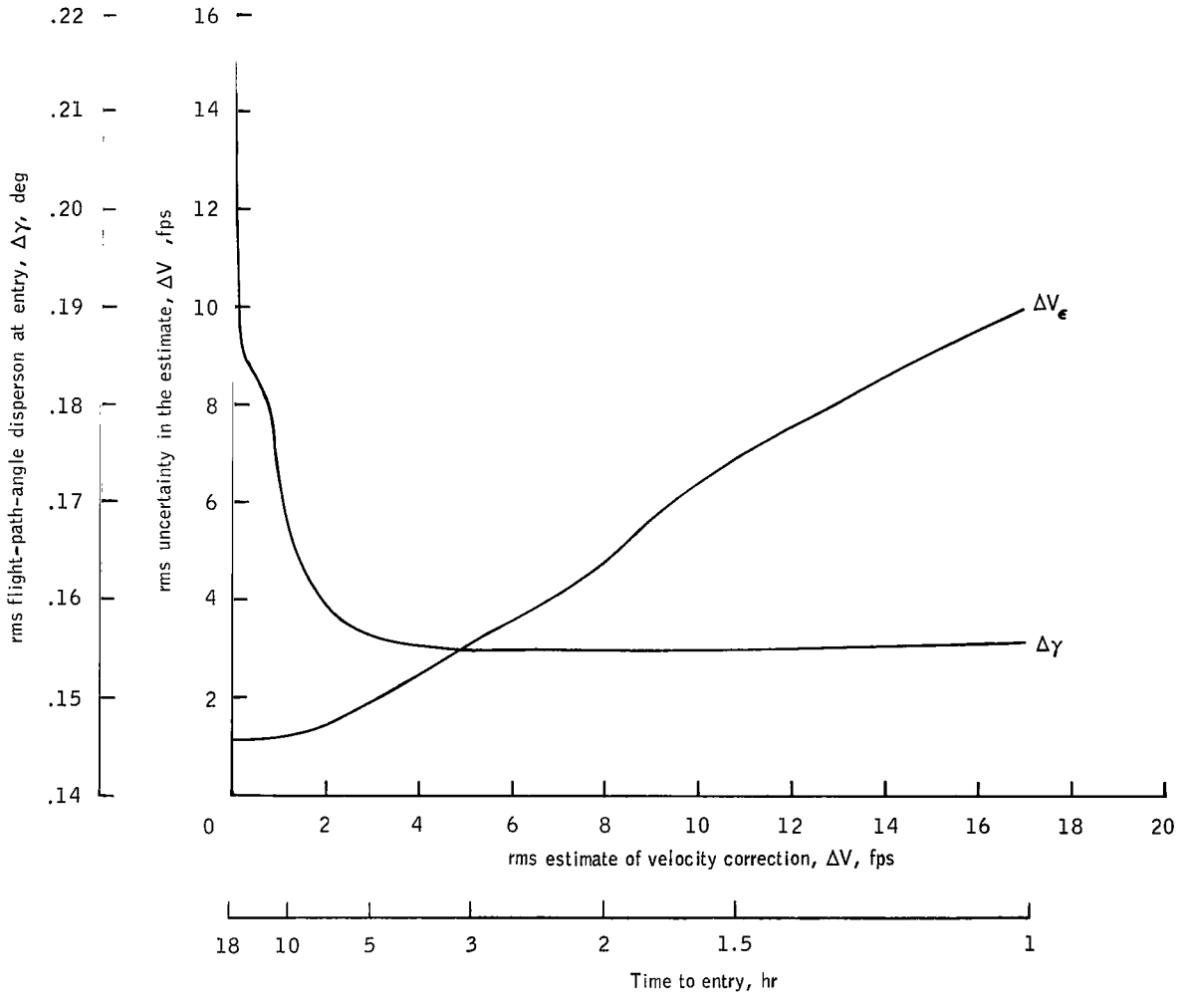

(b) Short-long trajectory; $E(t_0)$, $X(t_0)$ generated from Earth-based radar and onboard tracking.

Figure 5. - Continued.

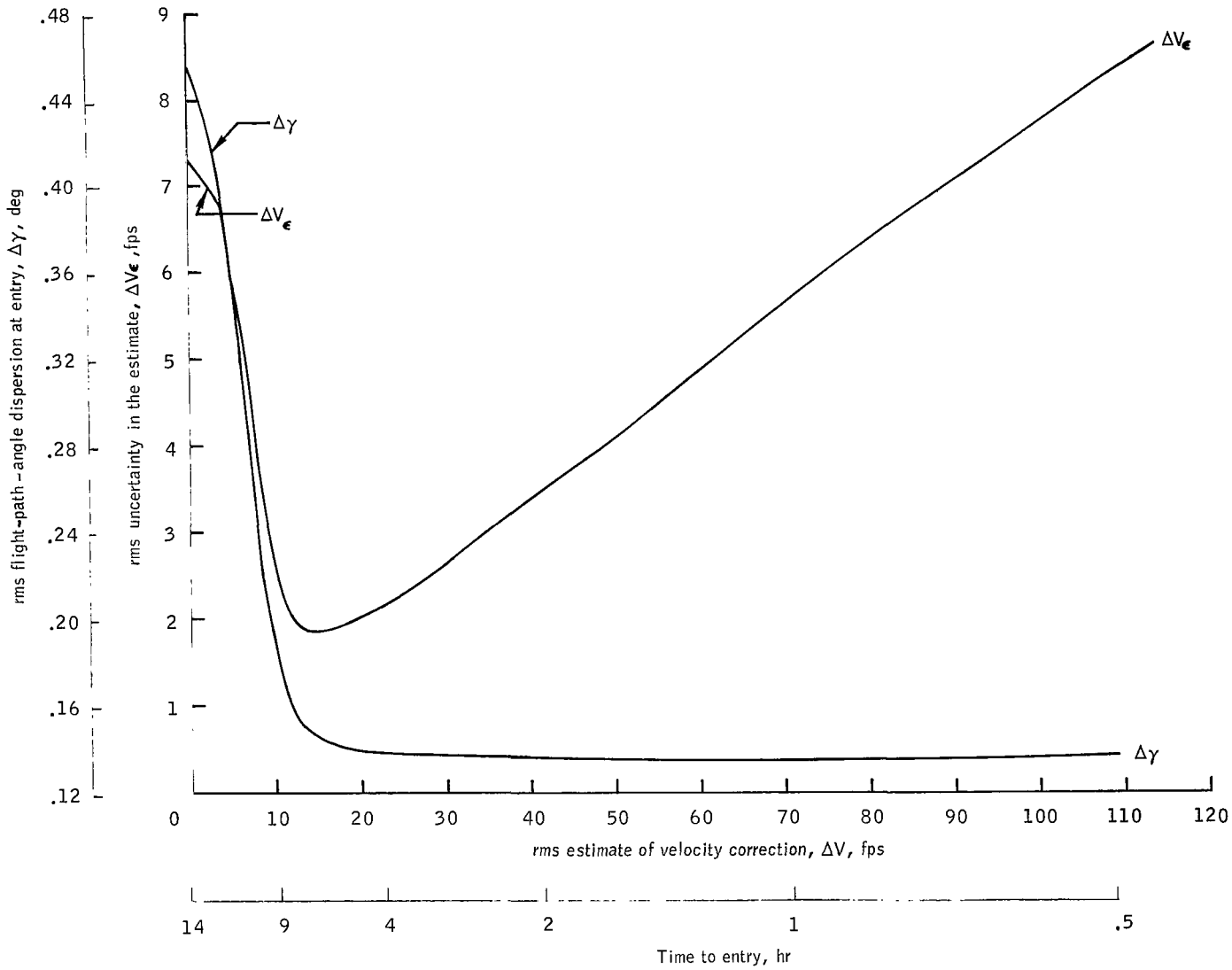

(c) Long-short trajectory; $E(t_0)$, $X(t_0)$ generated from Earth-based radar tracking only.

Figure 5. - Continued.

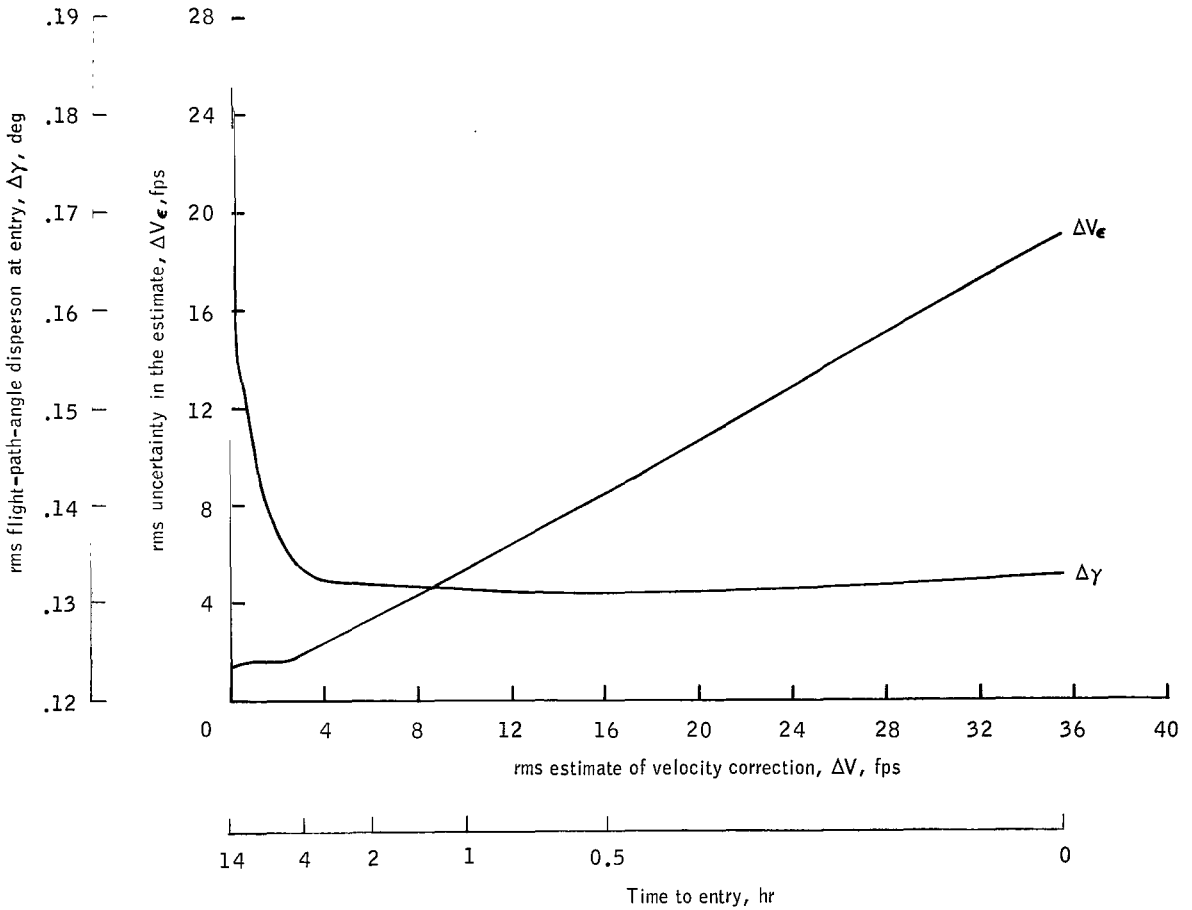

(d) Long-short trajectory; $E(t_0)$, $X(t_0)$ generated from Earth-based radar and onboard tracking.

Figure 5. - Concluded.

APPENDIX A

NAVIGATION SYSTEM EQUATIONS

The material developed in this appendix can generally be found in references 3 to 5. For onboard spacecraft navigation during a Mars flyby mission, the principal types of measurements that can be made are optical determinations of an angle. In this study, two optical instruments — the sextant and the theodolite — were considered.

In simulating the use of the sextant, measurements were made of the star-planet included angle. For each observation, a star was chosen randomly from an abbreviated catalog of stars incorporated in the simulation program. No attempt was made to optimize the selection of the star used. Since the study originates at and terminates in the Mars SOI, the observed planet was always Mars. Similarly, for the theodolite measurement, the planet Mars was always the observed body.

For each measurement, it is necessary to compute the H matrix, that is, the matrix of partial derivatives which relate measurement deviations to state deviations. The H matrix is associated with each type of observation and is expressed by

$$H(t) = \nabla_{\underline{S}} Q \tag{A1}$$

where Q is the measurable.

Sextant

For the sextant measurement, Q is the star-planet included angle β, and H(t) is a seven-dimensional vector expressed by

$$H(t)^T = \left[\frac{\partial \beta}{\partial \underline{r}_{vp}} \quad \frac{\partial \beta}{\partial \underline{v}_{vp}} \quad 1 \right] \tag{A2}$$

where the 1 component is representative of the derivative of the observable with respect to an associated bias, the component $\partial\beta/\partial\underline{v}_{vp} = 0$, and the component $\partial\beta/\partial\underline{r}_{vp}$ is derived by treating the star-planet included-angle measurement as a special case of the Sun-planet measurement (ref. 5). The geometry of the star-planet included-angle measurement is shown in figure 2.

Thus, assuming a vehicle-star vector $\underline{r}_s$ and a vehicle-planet vector $\underline{r}_{vp}$ for the derivation, the equation for the included angle β can be expressed by

$$\cos \beta = \frac{\underline{r}_{vp} \cdot \underline{r}_s}{|r_{vp}||r_s|} \tag{A3}$$

By taking first-order deviations of equation (A3), expanding the obtained form, and passing to the limit of the increasing r_s, the following equation for the star-planet included-angle measurement can be obtained.

$$\delta\beta = \frac{\partial\beta}{\partial \underline{r}_{vp}} \delta \underline{r}_{vp} = \left[\frac{\underline{u}_s - (\underline{u}_s \cdot \underline{u}_{vp}) \underline{u}_{vp}}{|r_{vp}| \sin \beta} \right] \cdot \delta \underline{r}_{vp} \tag{A4}$$

where $\underline{u}_s$ and $\underline{u}_{vp}$ are the unit vectors from the spacecraft to the star and to the planet, respectively.

From equation (A4), $\partial\beta/\partial \underline{r}_{vp}$ is obtained; consequently, H(t) for the star-planet included-angle measurement is completed.

Theodolite

For the theodolite measurement, Q would be the measurables, celestial latitude and longitude, of the observed body (denoted by β_1 and β_2, respectively), and H(t) would be an 8-by-2 matrix expressed by

$$H(t)^T = \begin{bmatrix} \dfrac{\partial\beta_1}{\partial \underline{r}_{vp}} & \dfrac{\partial\beta_1}{\partial \underline{v}_{vp}} & 1 & 0 \\ \dfrac{\partial\beta_2}{\partial \underline{r}_{vp}} & \dfrac{\partial\beta_2}{\partial \underline{v}_{vp}} & 0 & 1 \end{bmatrix} \tag{A5}$$

In this equation as in equation (A2), the derivatives of the observables with respect to the velocity and with respect to an associated bias would equal 0 and 1, respectively. The derivative with respect to the position is expressed by

$$\begin{bmatrix} \frac{\partial \beta_1}{\partial \underline{r}_{vp}} \\ \frac{\partial \beta_2}{\partial \underline{r}_{vp}} \end{bmatrix} = \begin{bmatrix} \frac{xz}{R^2 R'} & \frac{yz}{R^2 R'} & \frac{z^2 - R^2}{R^2 R'} \\ -\frac{y}{R'^2} & \frac{x}{R'^2} & 0 \end{bmatrix} \tag{A6}$$

where x, y, and z are components of the vector from the vehicle to the observed body, $R = \sqrt{x^2 + y^2 + z^2}$, and $R' = \sqrt{x^2 + y^2}$ (appendix C of ref. 3).

As a result of the navigation measurement and, consequently, of the evaluation of the sensitivity matrix H, knowledge of the vehicle state can be improved by using the information obtained to update the covariance matrix of state uncertainties E which is propagated along the trajectory by the equation

$$E(t) = \phi(t, t_0) E(t_0) \phi(t, t_0)^T \tag{A7}$$

where $\phi(t, t_0)$ is the state-transition matrix evaluated between t_0 and t. To insure that E(t) remains at least positive semidefinite, E is replaced in the propagation procedure by a matrix W so that

$$E(t) = W(t)W(t)^T \tag{A8}$$

The replacement of E by W is used only in the propagation procedure and not in the updating procedure.

When a measurement is made, the updated value of the E matrix is calculated from

$$E(t)^+ = E(t)^- - K(t)H(t)E(t)^- \tag{A9}$$

The weighting matrix K(t) is chosen so that the mean-squared position and velocity uncertainties are simultaneously minimized,

$$K(t) = E(t)^{-}H(t)^{T}M(t)^{-1} \tag{A10}$$

where

$$M(t) = H(t)E(t)^{-}H(t)^{T} + R(t) \tag{A11}$$

The covariance matrix of measurement errors R(t) is considered, for this study, to have four components: (1) error in the instrument, (2) error in the knowledge of the radius of the observed planet, (3) error associated with instrument bias, and (4) error caused by the uncertainty in the observed position of the planet. However, since the observed planet is the central body for the conic section, the last error component is zero (ref. 4), and consideration is given to only the first three error components. For the sextant measurements, R(t) is a scalar, and for the theodolite measurements, R(t) is a 2-by-2 matrix.

The first component to be considered is the variance of the optical instrument σ_I^2, which is already known. The second error component, the lack of knowledge of the radius of the observed planet, is inversely proportional to the distance of the planet from the vehicle. Thus, the change in θ (one-half the angle subtended by the observed planet) must be considered.

Referring to figure 2 for the geometry used in the derivation of the second error component of R(t)

$$\sin\theta = \frac{r_p}{|r_{vp}|} \tag{A12}$$

By taking deltas of the above equation and making the appropriate substitutions, the following equation is obtained.

$$\delta\theta = \tan\theta \frac{\delta r_p}{r_p} \tag{A13}$$

from which the parameter c is defined as the ratio of the planet-radius error to the radius of the observed planet, or

$$c = \frac{\delta r_p}{r_p} \tag{A14}$$

The third component, error associated with instrument bias, is given an initial value and is then estimated in the filter along with the state variable.

Thus, the total-variance equation of observation errors can be expressed as

$$R(t) = \sigma_T^2 = \left(\sigma_I^2 + c^2 \tan^2\theta + \sigma_B^2\right) I \tag{A15}$$

APPENDIX B

SOLUTION FOR THE CONIC TRAJECTORY THAT SATISFIES THE TERMINAL ENTRY CONDITIONS OF v_E, γ_E, h_E

The material presented in this appendix is based in part on reference 5. It is assumed that the probe is at the initial position vector $\underline{r}_0$ and that it is desired that the terminal or entry speed v_E, flight-path angle γ_E, and altitude h_E, be satisfied. The inclination i of the trajectory is specified. The geometry of this problem is shown in figure B-1. The velocity required $\underline{v}_R \left(\underline{v}_R = \underline{v}_{PROBE}\right)$ at t_0 to satisfy these conditions will now be derived.

The semimajor axis of the trajectory is computed from

$$a = \left(\frac{2}{r_E} - \frac{v_E^2}{\mu} \right)^{-1} \tag{B1}$$

where $r_E = h_E + r_p$. If $a > 0$, the trajectory is elliptic; if $a < 0$, the trajectory is hyperbolic.

The parameter p is found from

$$p = \frac{v_E^2 r_E^2 \sin^2 \gamma_E}{\mu} \tag{B2}$$

The eccentricity of the trajectory is then

$$e = \sqrt{1 - \frac{p}{a}} \tag{B3}$$

The radius of periapsis is found from

$$r_\pi = a(1 - e) \tag{B4}$$

It should be noted that if the trajectory is elliptical, the constraint

$$r_0 \leq 2a - r_\pi \tag{B5}$$

must be imposed.

From the polar equation of the orbit, the angle θ between $\underline{r}_0$ and $\underline{r}_E$ may be found from the true anomalies

$$f_0 = \cos^{-1}\left[\frac{1}{e}\left(\frac{p}{r_0} - 1\right)\right] \tag{B6}$$

and

$$f_E = \cos^{-1}\left[\frac{1}{e}\left(\frac{p}{r_E} - 1\right)\right] \tag{B7}$$

by setting

$$\theta = f_E - f_0 \tag{B8}$$

The normal to the trajectory plane is computed from

$$\underline{u}_h = \sin \Omega \sin i \, \underline{u}_x - \cos \Omega \sin i \, \underline{u}_y + \cos i \, \underline{u}_z \tag{B9}$$

The inclination i is specified, and Ω is the right ascension of the ascending node which may be computed from $\underline{r}_0$ and i, except for an ambiguity which may be freely chosen.

From figure B-2, the right ascension α_0 and declination δ_0 of $\underline{r}_0$ may be computed from

$$\alpha_0 = \tan^{-1}\left(\frac{y_0}{x_0}\right) \tag{B10}$$

and

$$\delta_0 = \sin^{-1}\left(\frac{z_0}{r_0}\right) \tag{B11}$$

Also from figure B-2

$$\Omega = \alpha_0 - \sigma \tag{B12}$$

for one choice of Ω, or

$$\Omega = \alpha_0 + \sigma + \pi \tag{B13}$$

for the other choice of Ω. For both cases, σ is computed from

$$\sin \sigma = \frac{\tan \delta_0}{\tan i} \tag{B14}$$

Equation (B14) implies the limits on the inclination which must be specified to make the equation meaningful; that is

$$\left|\tan i\right| > \left|\tan \delta_0\right| \tag{B15}$$

From figure B-1, it is evident that the entry position and velocity may be written

$$\underline{r}_E = r_E\left(\cos \theta \frac{\underline{r}_0}{r_0} + r_E \sin \theta \, \underline{u}_w\right) \tag{B16}$$

and

$$\underline{v}_E = v_E\left[\cos(\theta + \gamma_E)\frac{\underline{r}_0}{r_0} + v_E \sin(\theta + \gamma_E)\underline{u}_w\right] \tag{B17}$$

where the unit vector $\underline{u}_w$ lies in the trajectory plane and is defined by

$$\underline{u}_w = \underline{u}_h \times \underline{u}_{r_0} \tag{B18}$$

The velocity required may now be found simply from the triple crossproduct

$$\underline{r}_0 \times (\underline{r}_0 \times \underline{v}_R) = \underline{r}_0 \times (\underline{r}_E \times \underline{v}_E) \tag{B19}$$

which is true since $\underline{r}_0 \times \underline{v}_R = \underline{r}_E \times \underline{v}_E$ is the angular-momentum vector which must remain constant. After considerable algebra, equation (B19) may be solved for $\underline{v}_R$ as follows.

$$\underline{v}_R = \frac{\underline{r}_0}{r_0} v_0 \cos \gamma_0 + \underline{u}_w \frac{r_E v_E}{r_0} \sin \gamma_E \tag{B20}$$

The magnitude of $\underline{v}_R$ is found from

$$v_R^2 = \mu\left(\frac{2}{r_0} - \frac{1}{a}\right) \tag{B21}$$

The initial flight-path angle γ_0 may be found from

$$\left|\underline{r}_0 \times \underline{v}_R\right| = \left|\underline{r}_E \times \underline{v}_E\right| \tag{B22}$$

or

$$\left.\begin{aligned} r_0 v_R \sin \gamma_0 &= r_E v_E \sin \gamma_E \\ \gamma_0 &= \sin^{-1}\left(\frac{r_E v_E \sin \gamma_E}{r_0 v_R}\right) \end{aligned}\right\} \tag{B23}$$

The time to entry may be computed from the equation

$$\sqrt{\mu}\, t_E = \frac{\underline{r}_0 \cdot \underline{v}_R}{\sqrt{\mu}} X^2 C(\alpha X^2) + (1 - r_0 \alpha) X^3 S(\alpha X^2) + r_0 X \tag{B24}$$

where $\alpha = 1/a$ and $C(\alpha X^2)$ and $S(\alpha X^2)$ are Battin's auxiliary functions. The value X is found from

$$X = \frac{(E_E - E_0)}{\sqrt{\alpha}} \tag{B25}$$

if $a > 0$, and from

$$X = \frac{(H_E - H_0)}{\sqrt{-\alpha}} \tag{B26}$$

if $a < 0$. If the trajectory is elliptical ($a > 0$), the quantities E_E and E_0 are the eccentric anomalies and are found from

$$\tan\left(\frac{E}{2}\right) = \sqrt{\frac{1 - e}{1 + e}} \tan\left(\frac{f}{2}\right) \tag{B27}$$

If the trajectory is hyperbolic ($a < 0$), the quantities H_E and H_0 are found from

$$\tanh\left(\frac{H}{2}\right) = \sqrt{\frac{e - 1}{e + 1}} \tan\left(\frac{f}{2}\right) \tag{B28}$$

When these equations are applied to determine the $\underline{v}_R$ of the probe, the inclination and right ascension of the ascending node are the same, or very nearly the same, as those of the spacecraft.

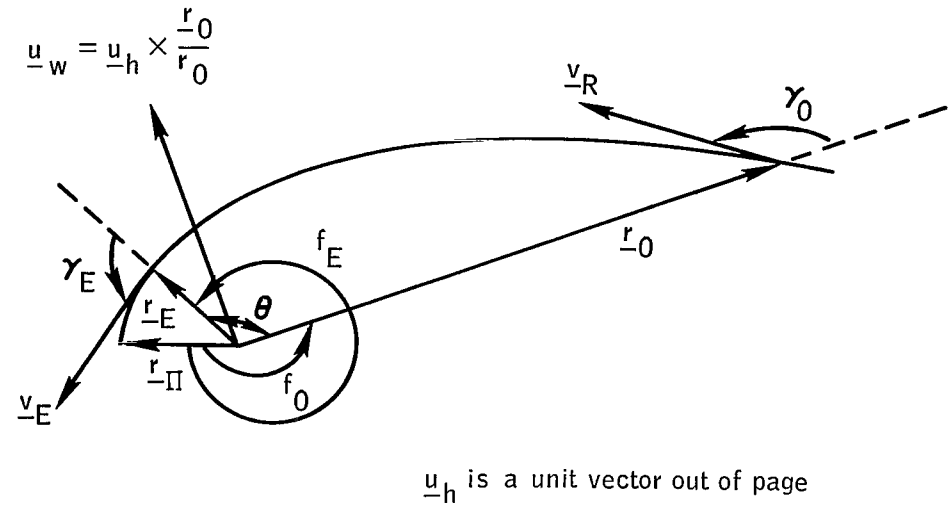

Figure B-1. - Geometry of trajectory which satisfies the entry conditions v_E, γ_E, $r_E = r_p + h_E$.

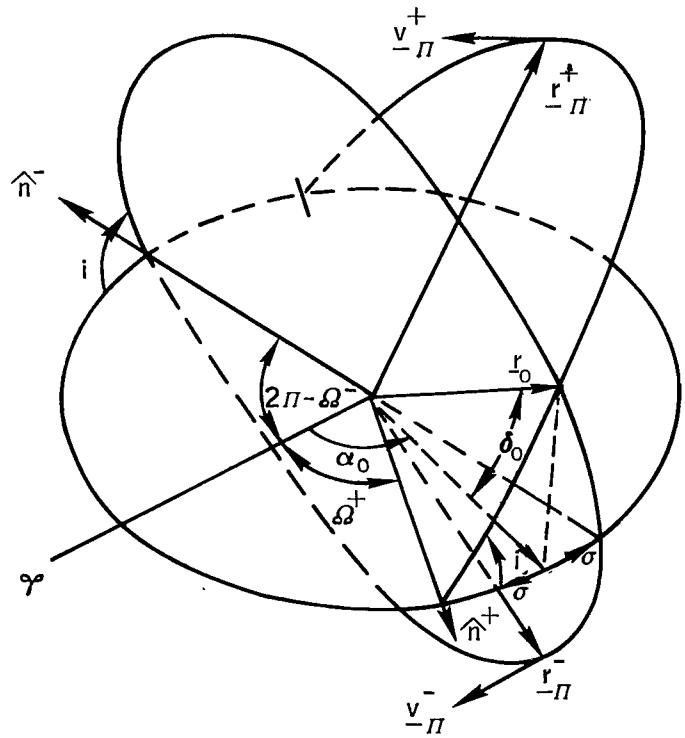

$$\Omega^- = \alpha + \sigma + \Pi$$
$$\Omega^+ = \alpha - \sigma$$
$$\sin \sigma = \frac{\tan \delta}{\tan i}$$

Figure B-2. - Geometry of the two trajectories possible that satisfy the entry conditions.

APPENDIX C

GUIDANCE SYSTEM ERROR EQUATIONS

The material presented in this appendix may be found in references 4 and 5. To perform a complete statistical evaluation of a guided flight, it is necessary to propagate and update the covariance matrix of the state uncertainties $E(t)$ and the covariance matrix of the state dispersions $X(t)$. Both matrices are propagated using the equations

$$E(t) = \phi(t, t_0) E(t_0) \phi(t, t_0)^T \tag{C1}$$

and

$$X(t) = \phi(t, t_0) X(t_0) \phi(t, t_0)^T \tag{C2}$$

where $\phi(t, t_0)$ is the state-transition matrix evaluated between t_0 and t. If a navigation measurement is made at time t, the matrix $X(t)$ remains unchanged. However, if a guidance correction is commanded, then both $E(t)$ and $X(t)$ are updated according to the following equations (ref. 5).

$$E(t)^+ = E(t)^- + BN(t)B^T \tag{C3}$$

and

$$X(t)^+ = [I + G(t)] \left[X(t)^- - E(t)^-\right] [I + G(t)]^T + E(t)^+ \tag{C4}$$

The 6-by-3 matrix B is defined by

$$B = \begin{pmatrix} 0 \\ I \end{pmatrix} \tag{C5}$$

where I is a 3-by-3 identity matrix. The 6-by-6 guidance matrix G(t) is written

$$G(t) = \begin{bmatrix} 0 & 0 \\ G_1(t) & G_2(t) \end{bmatrix} \tag{C6}$$

The derivations of the submatrices $G_1(t)$ and $G_2(t)$ for the analysis are presented in appendix D.

The matrix N(t) is defined as the covariance matrix of the velocity-correction error and is derived and discussed in references 4 and 5. The difference between the two derivations is that in reference 5 it is assumed that the inaccuracy in establishing a commanded velocity vector is caused only by random errors in thrust-vector orientation and magnitude. Reference 4 includes a third random error, designated as an engine-cutoff error. In this study, N(t) is used as derived in reference 4 and may be written as

$$N(t) = \overline{\zeta^2} L(t) + \frac{1}{2}\overline{\eta^2}\,[\ell(t) I - L(t)] + \frac{\overline{\epsilon^2} L(t)}{\ell(t)} \tag{C7}$$

where

$$L(t) = \begin{bmatrix} G_1(t) & G_2(t) \end{bmatrix} [\, X(t) - E(t)\,] \begin{bmatrix} G_1(t) & G_2(t) \end{bmatrix}^T \tag{C8}$$

and

$$\ell(t) = \text{trace } L(t) \tag{C9}$$

The parameters $\overline{\zeta^2}$, $\overline{\eta^2}$, and $\overline{\epsilon^2}$ are the mean-squared values of the errors in thrust magnitude, orientation, and cutoff, respectively. The rms estimate of the velocity correction is computed from equation (C8). The rms uncertainty in this estimate is computed from

$$P(t) = \begin{bmatrix} G_1(t) & G_2(t) \end{bmatrix} E(t) \begin{bmatrix} G_1(t) & G_2(t) \end{bmatrix}^T \tag{C10}$$

APPENDIX D

DISCUSSION OF GUIDANCE FOR FIXED TIME OF ARRIVAL AND FOR VARIABLE TIME OF ARRIVAL

A small velocity correction is to be made at time t to a trajectory to guarantee that certain terminal conditions will be met. Two general classes of terminal constraints which may be considered are fixed time of arrival (FTA) constraints and variable time of arrival (VTA) constraints. This appendix is an interpretation of FTA and VTA guidance presented in references 6 and 7, but the final results are obtained in terms of the familiar state-transition matrix. A particular application of VTA guidance, the guidance-to-entry nulling flight-path-angle errors which are not discussed in these references, is also presented.

At the instant before the velocity correction, the terminal position $\underline{r}_T^-$ is related to the position and velocity just prior to correction time by

$$\underline{r}_T^- = \underline{r}_T^-\left(\underline{r}^-, \underline{v}^-\right) \tag{D1}$$

Lack of a subscript on $\underline{r}$ and $\underline{v}$ means that they are evaluated at correction time t; a subscript T means that they are evaluated at the terminal time T.

Taking linear deviations of equation (D1) gives

$$\delta\underline{r}_T^- = \frac{\partial \underline{r}_T^-}{\partial \underline{r}^-}\delta r^- + \frac{\partial \underline{r}_T^-}{\partial \underline{v}^-}\delta \underline{v}^- \tag{D2}$$

At the instant after the velocity correction, the terminal position $\underline{r}_T^+$ is related to the position and velocity immediately after correction time by

$$\underline{r}_T^+ = \underline{r}_T^+\left(\underline{r}^+, \underline{v}^+\right) \tag{D3}$$

Taking linear deviations of equation (D3) gives

$$\delta \underline{r}_T^{+} = \frac{\partial \underline{r}_T^{+}}{\partial \underline{r}^{+}} \delta \underline{r}^{+} + \frac{\partial \underline{r}_T^{+}}{\partial \underline{v}^{+}} \delta \underline{v}^{+} \tag{D4}$$

Since there can be no instantaneous change in position, $\underline{r}^{+} = \underline{r}^{-} = \underline{r}$, and

$$\delta \underline{r}^{+} = \delta \underline{r}^{-} = \delta \underline{r} \tag{D5}$$

If the correction is assumed to be small and the trajectories are linearly related

$$\frac{\partial \underline{r}_T^{-}}{\partial \underline{r}^{-}} = \frac{\partial \underline{r}_T^{+}}{\partial \underline{r}^{+}} \tag{D6}$$

and

$$\frac{\partial \underline{r}_T^{-}}{\partial \underline{v}^{-}} = \frac{\partial \underline{r}_T^{+}}{\partial \underline{v}^{+}} \tag{D7}$$

These partials are the submatrices ϕ_{11} and ϕ_{12} of the state-transition matrix. (For the conic case, these are given in part in ref. 5.) Equations (D2) and (D4) may be written, using these simplifications, as

$$\delta \underline{r}_T^{-} = \phi_{11} \delta \underline{r} + \phi_{12} \delta \underline{v}^{-} \tag{D8}$$

and

$$\delta \underline{r}_T^{+} = \phi_{11} \delta \underline{r} + \phi_{12} \delta \underline{v}^{+} \tag{D9}$$

Note that $\delta\underline{v}^-$ and $\delta\underline{v}^+$ are related to the nominal trajectory by

$$\delta\underline{v}^- = \underline{v}^- - \underline{v}_{nom} \tag{D10}$$

and

$$\delta\underline{v}^+ = \underline{v}^+ - \underline{v}_{nom} \tag{D11}$$

The velocity-correction vector $\Delta\underline{v}$ is found from

$$\left.\begin{aligned} \Delta\underline{v} &= \underline{v}^+ - \underline{v}^- \\ \text{or} \\ \Delta\underline{v} &= \delta\underline{v}^+ - \delta\underline{v}^- \end{aligned}\right\} \tag{D12a}$$

Now, solving equation (D8) for δv^- and equation (D9) for $\delta\underline{v}^+$, and by differencing the results, $\Delta\underline{v}$ is obtained as

$$\Delta\underline{v} = \phi_{12}^{-1}\left(\delta\underline{r}_T^+ - \delta\underline{r}_T^-\right) \tag{D12b}$$

Replacing $\delta\underline{r}_T^-$ by equation (D8), $\Delta\underline{v}$ becomes

$$\Delta\underline{v} = \phi_{12}^{-1}\left(\delta\underline{r}_T^+ - \phi_{11}\delta\underline{r} - \phi_{12}\delta\underline{v}^-\right) \tag{D13}$$

FTA Guidance

In this type of guidance, it is desired to null the position deviations $\delta\underline{r}_T^+$ at the fixed terminal time T, that is

$$\underline{\delta r}_T^{+} = 0 \tag{D14}$$

Then $\Delta\underline{v}$ becomes

$$\left.\begin{aligned} \Delta\underline{v}_F &= -\phi_{12}^{-1}\phi_{11}\underline{\delta r} - \underline{\delta v}^{-} \\ \text{or} \\ \Delta\underline{v}_F &= G_1\underline{\delta r} + G_2\underline{\delta v}^{-} \end{aligned}\right\} \tag{D15}$$

where

$$\left.\begin{aligned} G_1 &= -\phi_{12}^{-1}\phi_{11} \\ G_2 &= -I \end{aligned}\right\} \tag{D16}$$

VTA Guidance

In this type of guidance, the terminal time T is allowed to be free. For example, let the component of the position deviation parallel to the velocity at T be given by

$$\underline{\delta r}_T^{+} = -\underline{v}_T\delta T \tag{D17}$$

Substituting into equation (D13), $\Delta\underline{v}$ for VTA is given by

$$\Delta\underline{v}_V = \phi_{12}^{-1}\left(-\underline{v}_T\delta T - \phi_{11}\underline{\delta r} - \phi_{12}\underline{\delta v}\right) \tag{D18}$$

The VTA correction can then be expressed in terms of the FTA correction as

$$\Delta\underline{v}_V = \Delta\underline{v}_F - \phi_{12}^{-1}\underline{v}_T\delta T \tag{D19}$$

By defining

$$\underline{W} = \phi_{12}^{-1} \underline{v}_T \tag{D20}$$

equation (D19) becomes

$$\Delta \underline{v}_V = \Delta \underline{v}_F - \underline{W}\, \delta T \tag{D21}$$

Since there is an additional degree of freedom remaining, δT may be chosen, if desired, to minimize $\Delta \underline{v}_V$. From equation (D21)

$$\left.\begin{aligned} \Delta v_V^2 &= \Delta v_F^2 - 2\underline{W} \cdot \Delta \underline{v}_F\, \delta T + \underline{W} \cdot \underline{W}\, \delta T^2 \\ \text{and} \\ \frac{\partial\left(\Delta v_V^2\right)}{\partial(\delta T)} &= -2\underline{W} \cdot \Delta \underline{v}_F + 2\underline{W} \cdot \underline{W}\, \delta T = 0 \\ \text{or} \\ \delta T &= -\frac{\underline{W} \cdot \Delta \underline{v}_F}{\underline{W} \cdot \underline{W}} \end{aligned}\right\} \tag{D22}$$

Substituting back into equation (D21)

$$\Delta \underline{v}_V = \left(I - \frac{\underline{W}\ \underline{W}^T}{\underline{W} \cdot \underline{W}}\right) \Delta \underline{v}_F = G_1 \delta \underline{r} + G_2 \delta \underline{v} \tag{D23}$$

where

$$\left.\begin{aligned} G_1 &= -\left(I - \frac{\underline{W}\,\underline{W}^T}{\underline{W}\cdot\underline{W}}\right)\phi_{12}^{-1}\phi_{11} \\ G_2 &= -\left(I - \frac{\underline{W}\,\underline{W}^T}{\underline{W}\cdot\underline{W}}\right) \end{aligned}\right\} \tag{D24}$$

VTA Guidance, Null $\delta\gamma_T$

The extra degree of freedom in VTA guidance may also be used to control an additional terminal deviation if desired. As an example, the errors in flight-path angle at the terminal time may be nulled.

The deviation in flight-path angle is shown in appendix E to be a function of position and velocity deviations at T such that

$$\delta\gamma_T = \underline{Z}_1^T \delta\underline{r}_T^+ + \underline{Z}_2^T \delta\underline{v}_T^+ \tag{D25}$$

But

$$\delta\underline{r}_T^+ = \phi_{11}\delta\underline{r} + \phi_{12}\delta\underline{v}^+ \tag{D9}$$

and

$$\delta\underline{v}_T^+ = \phi_{21}\delta\underline{r} + \phi_{22}\delta\underline{v}^+ \tag{D26}$$

Solving these two equations for $\delta\underline{v}_T^+$ and eliminating $\delta\underline{v}^+$

$$\delta\underline{v}_T^+ = \phi_{21}\delta\underline{r} + \phi_{22}\phi_{12}^{-1}\left(\delta\underline{r}_T^+ - \phi_{11}\delta\underline{r}\right) \tag{D27a}$$

or

$$\delta \underline{v}_T^+ = \left(\phi_{21} - \phi_{22}\phi_{12}^{-1}\phi_{11}\right)\delta \underline{r} + \phi_{22}\phi_{12}^{-1}\delta \underline{r}_T^+ \tag{D27b}$$

Substituting this equation into equation (D25) to eliminate $\delta \underline{v}_T^+$

$$\delta\gamma_T = \left(\underline{Z}_1^T + \underline{Z}_2^T\phi_{22}\phi_{12}^{-1}\right)\delta \underline{r}_T^+ + \underline{Z}_2^T\left(\phi_{21} - \phi_{22}\phi_{12}^{-1}\phi_{11}\right)\delta \underline{r} \tag{D28}$$

Using equation (D17), setting $\delta\gamma_T = 0$, and solving for δT yields

$$\delta T = \frac{\underline{Z}_2^T\left(\phi_{21} - \phi_{22}\phi_{12}^{-1}\phi_{11}\right)\delta \underline{r}}{\left(\underline{Z}_1^T + \underline{Z}_2^T\phi_{22}\phi_{12}^{-1}\right)\underline{v}_T} \tag{D29}$$

This equation is the time deviation required for the deviation in flight-path angle to be nulled. Substituting equation (D29) into equation (D18)

$$\left(\Delta \underline{v}_V\right)_{\delta\gamma_T=0} = G_1\delta \underline{r} + G_2\delta \underline{v} \tag{D30}$$

where

$$\left.\begin{aligned} G_1 &= -\frac{\phi_{12}^{-1}\underline{v}_T\,\underline{Z}_2^T\left(\phi_{21} - \phi_{22}\phi_{12}^{-1}\phi_{11}\right)}{\left(\underline{Z}_1^T + \underline{Z}_2^T\phi_{22}\phi_{12}^{-1}\right)\underline{v}_T} - \phi_{12}^{-1}\phi_{11} \\ G_2 &= -I \end{aligned}\right\} \tag{D31}$$

These guidance laws are applied directly to the guidance-to-entry problem discussed in the body of this paper. The terminal conditions subscripted by T are the same as the entry conditions subscripted by E.

APPENDIX E

COMPUTATION OF ROOT-MEAN-SQUARE FLIGHT-PATH-ANGLE AND PERIAPSIS-RADIUS ERRORS

The basic equation which relates the flight-path angle γ to the position $\underline{r}$ and the velocity $\underline{v}$ is

$$\cos \gamma = \frac{\underline{r} \cdot \underline{v}}{rv} \tag{E1}$$

from which

$$\delta\gamma = \underline{Z}_1^T \delta\underline{r} + \underline{Z}_2^T \delta\underline{v} \tag{E2}$$

If the computation of the flight-path-angle error is desired for fixed time, then

$$\underline{Z}_1 = \frac{\underline{r} \times (\underline{r} \times \underline{v})}{r^2 |\underline{r} \times \underline{v}|} \tag{E3}$$

If the calculation requires flight-path-angle error for fixed radius, then

$$\underline{Z}_1 = -\frac{\underline{v}}{|\underline{r} \times \underline{v}|} \tag{E4}$$

In either case (fixed time or fixed radius), $\underline{Z}_2$ is written

$$\underline{Z}_2 = \frac{(\underline{r} \times \underline{v}) \times \underline{v}}{v^2 |\underline{r} \times \underline{v}|} \tag{E5}$$

Defining $\underline{Z}^T = \left(\underline{Z}_1^T \quad \underline{Z}_2^T\right)$, equation (E2) becomes

$$\delta\gamma = \underline{Z}^T \delta\underline{s} \tag{E6}$$

where

$$\delta\underline{s} = \begin{pmatrix} \delta\underline{r} \\ \delta\underline{v} \end{pmatrix} \tag{E7}$$

Therefore

$$\delta\gamma^2 = \underline{Z}^T \delta\underline{s} \delta\underline{s}^T \underline{Z} \tag{E8}$$

Taking expected values of equation (E8) gives

$$\xi\left(\delta\gamma^2\right) = \sigma_\gamma^2 = \underline{Z}^T \xi\left(\delta\underline{s}\delta\underline{s}^T\right)\underline{Z} \tag{E9}$$

Since X(t) is defined by $\xi\left(\delta\underline{s}\delta\underline{s}^T\right)$, the mean-squared flight-path-angle dispersion is computed from

$$\sigma_{\gamma d}^2 = \underline{Z}(t)^T \mathbf{X}(t) \underline{Z}(t) \tag{E10}$$

Similarly, the mean-squared flight-path-angle uncertainty can be computed from

$$\sigma_{\gamma u}^2 = \underline{Z}(t)^T \mathbf{E}(t) \underline{Z}(t) \tag{E11}$$

The derivation of the periapsis-radius errors can be computed by at least two methods. The first method is quite similar to that presented for the calculation of flight-path-angle errors and can be found in reference 4. The radius of periapsis can be

written as a function of the position and velocity at any point along the conic, from which

$$\delta r_\pi = \underline{y}_1^T \delta \underline{r} + \underline{y}_2^T \delta \underline{v} \tag{E12}$$

where

$$\underline{y}_1 = \frac{\partial r_\pi}{\partial r} \frac{\underline{r}}{r} + \frac{2(\underline{r} \cdot \underline{v})}{r^4} \frac{\partial r_\pi}{\partial v_H^2} \left[\underline{r} \times (\underline{r} \times \underline{v})\right] \tag{E13}$$

and

$$\underline{y}_2 = \frac{2}{r^2} \frac{\partial r_\pi}{\partial v_H^2} \left[(\underline{r} \times \underline{v}) \times \underline{r}\right] + 2 \frac{\partial r_\pi}{\partial v^2} \underline{v} \tag{E14}$$

In these equations, v_H is the down-range speed, and the required partial derivatives are computed with the following relations.

$$\frac{\partial r_\pi}{\partial r} = \frac{2ar_\pi}{r^2} - \frac{av_H^2}{e} \left(\frac{v^2 r}{\mu^2} - \frac{1}{\mu}\right) \tag{E15}$$

$$\frac{\partial r_\pi}{\partial v_H^2} = \frac{r^2}{2\mu e} \tag{E16}$$

and

$$\frac{\partial r_\pi}{\partial v^2} = \frac{ar_\pi}{\mu} - \frac{av_H^2}{2e\left(\frac{\mu}{r}\right)^2} \tag{E17}$$

where μ is the gravitational constant times the mass of the central body, and a and e are the semimajor axis and the eccentricity of the conic, respectively. If the

procedure outlined for computing flight-path-angle errors is used, equations similar to equations (E10) and (E11) can be written as

$$\left(\sigma_{r_{\pi u}}\right)^2 = \underline{y}(t)^T E(t) \underline{y}(t) \tag{E18}$$

for the mean-squared uncertainty in periapsis radius, and as

$$\left(\sigma_{r_{\pi d}}\right)^2 = \underline{y}(t)^T X(t) \underline{y}(t) \tag{E19}$$

for the mean-squared dispersion in periapsis radius.

The second method which can be used to compute the periapsis-radius errors requires the computation of the state-transition matrix between an arbitrary time t along the conic and the nominal time of periapsis passage T_π. For example, consider the computation of the radius-of-periapsis dispersion. A dispersion matrix at T_π is computed from

$$X\left(T_\pi\right) = \phi\left(T_\pi, t\right) X(t) \phi\left(T_\pi, t\right)^T \tag{E20}$$

and, if $A\left(T_\pi\right)$ represents the transformation from a planet-centered inertial coordinate system to a locally level coordinate system (described in the text of this paper), then

$$X'\left(T_\pi\right) = A\left(T_\pi\right) X\left(T_\pi\right) A\left(T_\pi\right)^T \tag{E21}$$

from which the rms radius-of-periapsis dispersion is obtained from

$$\sigma_{r_{\pi d}} = \sqrt{X_{11}'\left(T_\pi\right)} \tag{E22}$$

If E(t) replaces X(t) in equation (E20), the rms radius-of-periapsis uncertainty can be computed in a similar fashion.

REFERENCES

1. Cicolani, Luigi S. : Interplanetary Midcourse Guidance Using Radar Tracking and On-board Observation Data. NASA TN D-3623, 1966.

2. Lee, V. A. ; and Wilson, S. W., Jr. : A Survey of Ballistic Mars-Mission Profiles. J. Spacecraft Rockets, vol. 4, no. 2, Feb. 1967, pp. 129-142.

3. Smith, Gerald L. ; Schmidt, Stanley F. ; and McGee, Leonard A. : Application of Statistical Filter Theory to the Optimal Estimation of Position and Velocity on Board a Circumlunar Vehicle. NASA TR R-135, 1962.

4. White, John S. ; Callas, George P. ; and Cicolani, Luigi S. : Application of Statistical Filter Theory to the Interplanetary Navigation and Guidance Problem. NASA TN D-2697, 1965.

5. Battin, Richard H. : Astronautical Guidance. McGraw-Hill Book Co., Inc. (New York, N. Y.), 1964.

6. Stern, Robert Gottlieb: Interplanetary Midcourse Guidance Analysis. Ph. D. Dissertation, M. I. T., published as NASA CR-51827, 1963.

7. Cicolani, Luigi S. : Linear Theory of Impulsive Velocity Corrections for Space Mission Guidance. NASA TN D-3365, 1966.

"The aeronautical and space activities of the United States shall be conducted so as to contribute . . . to the expansion of human knowledge of phenomena in the atmosphere and space. The Administration shall provide for the widest practicable and appropriate dissemination of information concerning its activities and the results thereof."

—NATIONAL AERONAUTICS AND SPACE ACT OF 1958

NASA SCIENTIFIC AND TECHNICAL PUBLICATIONS

TECHNICAL REPORTS: Scientific and technical information considered important, complete, and a lasting contribution to existing knowledge.

TECHNICAL NOTES: Information less broad in scope but nevertheless of importance as a contribution to existing knowledge.

TECHNICAL MEMORANDUMS: Information receiving limited distribution because of preliminary data, security classification, or other reasons.

CONTRACTOR REPORTS: Scientific and technical information generated under a NASA contract or grant and considered an important contribution to existing knowledge.

TECHNICAL TRANSLATIONS: Information published in a foreign language considered to merit NASA distribution in English.

SPECIAL PUBLICATIONS: Information derived from or of value to NASA activities. Publications include conference proceedings, monographs, data compilations, handbooks, sourcebooks, and special bibliographies.

TECHNOLOGY UTILIZATION PUBLICATIONS: Information on technology used by NASA that may be of particular interest in commercial and other non-aerospace applications. Publications include Tech Briefs, Technology Utilization Reports and Notes, and Technology Surveys.

Details on the availability of these publications may be obtained from:

SCIENTIFIC AND TECHNICAL INFORMATION DIVISION

NATIONAL AERONAUTICS AND SPACE ADMINISTRATION

Washington, D.C. 20546